

# POLITECNICO DI TORINO

Corso di Laurea Magistrale  
in Nanotechnologies for ICTs

Tesi di Laurea Magistrale

Design and Synthesis of DNA Origami Biosensors  
for DNA and Protein Detection



Relatori:

prof. Paul W.K. Rothmund

prof. Valentina Cauda

prof. Carlo Ricciardi

Candidato:

Matteo Michele Guareschi

Anno Accademico 2018/2019







# Abstract

DNA nanotechnology is a promising technique for DNA and protein sensors, owing to its affinity to biological molecules and to the possibility of precisely tuning geometry and functions to optimize the actuation and signal transduction. Specifically, one can design two- and three-dimensional nanometric shapes with DNA origami, where a long DNA strand is folded by hybridization of shorter DNA strands. While a large variety of biosensing techniques exists, the versatility and programmability of DNA nanotechnology could make it a valid competitor in this field, overcoming some of the previous limitations. This project aims to demonstrate a DNA strand sensor that exploits DNA origami as the bioreceptor and redox indicators as transducers. Starting from existing systems fabricated using single DNA strands (EDNA), a characterization process is established, introducing electrochemical techniques for quantitative analysis, measuring probe density via cyclic voltammetry and electron transfer rate via square wave voltammetry. This is obtained by adapting previous methods to the new design, at the same time creating a point of reference for future systems. Through similar means and measurement techniques, we establish a fabrication process that is studied from the choice of substrate to the validation of each preparation step. Together with the active elements on the gold electrode, a passivation layer must be deposited to remove background currents. Several of such self-assembled monolayers are prepared and characterized, evaluating their interaction with DNA. A fundamental result is then heavily labelling DNA origami with redox active molecules, here methylene blue, in order to increase the current shift per single binding event, increasing contrast and signal amplification, two key parameters in any sensor. When DNA origami are folded under heavy loading conditions, the redox indicators cause them to aggregate, rendering them unusable. Several possible causes are hypothesized and tested, until successful labelling is obtained. The device is finally demonstrated in a proof of concept design that can perform sensing of short DNA strands through the detachment of methylene blue labelled DNA origami from a gold electrode, leading to a decrease in current proportional to the number of binding events. This sys-

---

tem is a first step in the desired direction and can further be expanded by use of different structures that will create a single molecule system, allowing for in vivo use, and that will be able to accommodate different analytes, such as larger proteins.

# Abstract

La nanotecnologia del DNA è una tecnica promettente per sensori per DNA e proteine, grazie alla sua affinità nei confronti di molecole biologiche e alla possibilità di perfezionarne geometria e funzioni per ottimizzare l'attuazione e la trasduzione del segnale. Lo scopo di questo progetto è di realizzare un sensore per frammenti di DNA che sfrutti DNA origami come biorecettore e indicatori redox come trasduttori. Partendo da sistemi già esistenti, fabbricati utilizzando singoli filamenti di DNA, è stato disegnato un processo di caratterizzazione, introducendo tecniche di elettrochimica per un'analisi quantitativa, misurando la densità di sensori insieme alle proprietà dinamiche del sistema. Questi metodi già esistenti sono stati adattati al nuovo sistema, creando allo stesso tempo un punto di riferimento per sistemi futuri. Attraverso mezzi e tecniche di misura simili, abbiamo stabilito un processo di fabbricazione che parte dalla scelta del substrato fino alla validazione di ogni passaggio durante la preparazione. Un risultato fondamentale è poi quello di funzionalizzare DNA origami con un alto numero di molecole elettrochimicamente attive, in questo caso blu di metilene, per aumentare il cambiamento di corrente ad ogni cattura di una molecola analizzata, migliorando il contrasto e l'amplificazione del segnale, due parametri chiave in ogni sensore. XXXX. Il dispositivo viene infine realizzato in una versione semplificata che può effettuare il rilevamento di piccoli frammenti di DNA attraverso il distacco da un elettrodo in oro di DNA origami funzionalizzati con blu metilene, portando a una diminuzione di corrente proporzionale al numero di eventi di cattura. Questo sistema è il primo passo nella direzione desiderata e verrà migliorato utilizzando una struttura diversa che creerà un sistema a singola molecola, permettendo l'uso in vivo, e che potrà rilevare molecole diverse e più grandi, come le proteine.



# Abstract

Les capteurs biologiques.

La nanotechnologie du DNA est une technique prometteuse pour capteurs d'ADN et de protéines, grâce à son affinité envers molécules biologiques et à la possibilité d'en perfectionner la géométrie et les fonctions pour optimiser l'actionnement et la transduction du signal. Le but de ce projet est d'accomplir un capteur pour fils d'ADN qu'exploite DNA origami comme biosenseurs et indicateurs rédox comme transducteurs. En commençant par des systèmes déjà existants, fabriqués avec d'ADN simple brin, on a conçu un procédé de caractérisation, en introduisant des techniques d'électrochimie pour des analyses quantitatives, avec la mesure de la densité des capteurs et des propriétés dynamiques du système. Ces procédés déjà existants ont été adaptés au nouveau système et en même temps on a créé un point de référence pour systèmes futurs. Par des similaires moyens et techniques de mesure, on a établi un procédé de fabrication que part du choix du substrat jusqu'à la validation de chaque passage pendant la préparation. Un résultat fondamental est ensuite le pouvoir de fonctionnaliser DNA origami avec un nombre élevé de molécules électrochimiquement actives, dans ce cas bleu de méthylène, pour augmenter le changement de courant pour chaque événement de liaison, pour améliorer le contraste et l'amplification du signal, deux paramètres clés pour tous les capteurs. XXXX. Le dispositif est enfin réalisé comme preuve de concept que peut détecter des courts fragments d'ADN par le détachement d'une électrode en or des DNA origami avec bleu de méthylène, menant à une diminution de courant proportionnelle au nombre des événements de liaison. Ce système est la première étape vers la direction souhaitée et il sera amélioré en utilisant une structure différente que créera un système a une molécule unique, permettant une utilisation in vivo, et que pourra aussi relever des molécules différentes et plus grand, comme des protéines.



# Contents

|          |   |           |
|----------|---|-----------|
| <b>1</b> | <b>Introduction</b>                                 | <b>1</b>  |
| 1.1      | DNA Nanotechnology . . . . .                        | 1         |
| 1.1.1    | DNA Origami . . . . .                               | 4         |
| 1.1.2    | DNA Strand Displacement . . . . .                   | 6         |
| 1.2      | Electrochemical Transduction . . . . .              | 6         |
| 1.2.1    | Measurement Setup . . . . .                         | 8         |
| 1.2.2    | Nonfaradaic and faradaic disturbances . . . . .     | 10        |
| 1.2.3    | Cyclic Voltammetry . . . . .                        | 12        |
| 1.2.4    | Alternating Current Voltammetry . . . . .           | 14        |
| 1.2.5    | Square Wave Voltammetry . . . . .                   | 15        |
| 1.2.6    | Impedance Spectroscopy . . . . .                    | 17        |
| 1.3      | Biological Sensors . . . . .                        | 19        |
| 1.3.1    | Enzyme-linked Immunosorbent Assay (ELISA) . . . . . | 20        |
| 1.3.2    | EDNA . . . . .                                      | 20        |
| 1.3.3    | DNA Origami Sensor Concept . . . . .                | 25        |
| <b>2</b> | <b>Preliminary Electrochemical Measurements</b>     | <b>29</b> |
| 2.1      | Stepwise Fabrication Control . . . . .              | 29        |
| 2.2      | Electroactive Area Estimation . . . . .             | 32        |
| 2.3      | Probe Density . . . . .                             | 36        |
| 2.4      | Electron Transfer Rate . . . . .                    | 39        |
| 2.5      | Surface Passivation . . . . .                       | 43        |
| <b>3</b> | <b>Labelling of DNA Origami with Methylene Blue</b> | <b>45</b> |
| 3.1      | Auxiliary Structure Design . . . . .                | 45        |

|          |   |           |
|----------|---|-----------|
| 3.2      | Death star design with 30 surface binding sites and 98 methylene blue sites | 47        |
| 3.2.1    | Annealing and purification of the origami                                   | 49        |
| 3.3      | Effects of Methylene Blue Density and Concentration                         | 52        |
| 3.4      | Reduction of Methylene Blue   | 56        |
| 3.5      | Changing the Number of Methylene Blue Sites                                 | 58        |
| <b>4</b> | <b>DNA Origami Electrochemical Sensor</b>                                   | <b>65</b> |
| 4.0.1    | Purification  | 67        |
| 4.1      | Origami Displacement  | 70        |
| <b>5</b> | <b>Conclusions</b>  | <b>73</b> |
| <b>6</b> | <b>Acknowledgements</b>   | <b>75</b> |

# Introduction

## 1.1 DNA Nanotechnology

The interest in DNA nanotechnology stems from its peculiar base-pair complementarity which precisely defines a map of a single strand that can be subsequently addressed by using the sequence complementary to the desired position. The hybridization of two perfectly matching DNA sequences forms the well known double helix shape, which does not have a fixed structure, but can fold and move. Holliday proposed one of the first modifications<sup>1</sup> of the double helix, theorizing the possible crossing of four partially complementary DNA strands that form a four-way intersection as shown in Figure 1.1. Such a structure not only links and holds together four different strands, but it gives them a definite secondary cross shape. This interlocking of strands was thought as a naturally occurring process in biological systems, not as an artificial modification and then further studies showed that this indeed happens in nature, for example in meiosis processes<sup>2</sup>.

Furthermore, the idea is applicable to synthesized DNA, giving birth to the field of DNA nanotechnology. When different DNA oligonucleotides are linked together by several junctions, more complex shapes are obtained and structural rigidity is added, so that there is no flexible double helix anymore, but structures that can be imaged consistently<sup>3</sup>. Using many strands also means that the formation of the final structure might be prevented by the failed hybridization of one strand that should link two different parts, no single strand acts as backbone for the structure, thus all of them are equally necessary. A different way to do so is to just one long (more than 1 kilobase) single strand that folds on itself and has internal complementary sequences that can hybridize to each other<sup>4</sup>. 3D designs can be obtained by using secondary structures that can interact to form tertiary

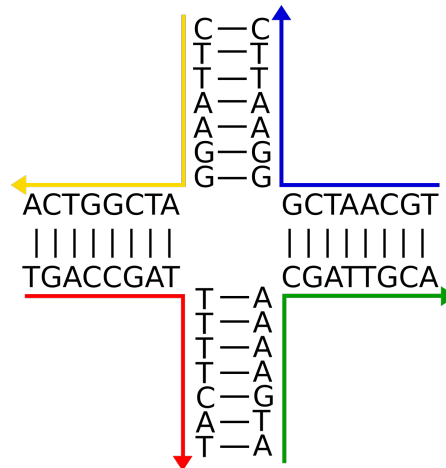


**Figure 1.1** – Four partially complementary DNA strands forming a Holliday junction.

foldings, such as the polyhedron shown in Figure 1.2.

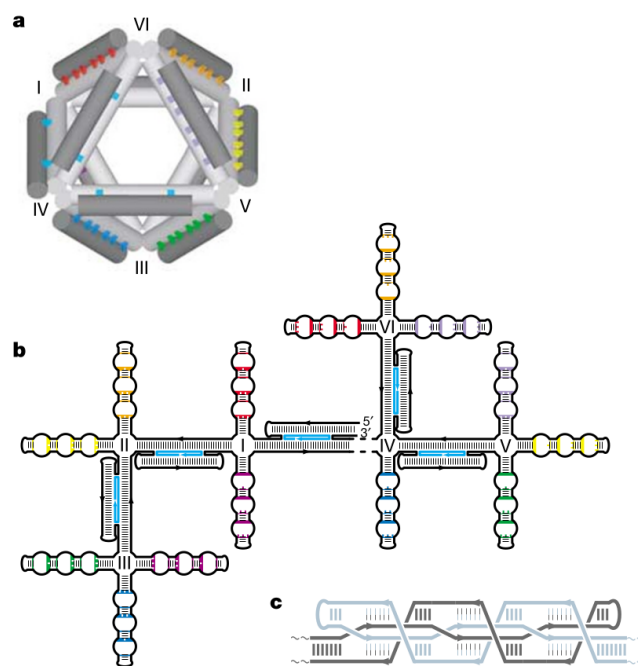


**Figure 1.2** – Single stranded DNA folding into a octahedron from [4]. a) final 3d structure of the polyhedron; b) planar structure before folding; c) interweaving of two of the DNA stem-loops shown in b). Reprinted by permission from Springer Nature: Nature [4], copyright 2004.

### 1.1.1 DNA Origami

After a few decades of research, in 2006 a method<sup>5</sup> was proposed to shape DNA in any two-dimensional connected shape. The idea is to use a several kilobase long scaffold strand, the sequence of which is well known, and fold it where needed by using shorter staples strands. These are aptamers with a length of 20-40 bases that will bind to the scaffold partly in a first location, partly in a second one, thus stapling the two positions together and folding what is between them. When this is done hundreds of times, progressively completing the double helix, the result can be shaped as desired, in simpler ways, similar to Figure 1.3, or with any connected design, for example as in Figure 1.4. The characteristic double helix shape of double stranded DNA forces a limitation on where two different double helices can be linked together by a staple strand: it must happen at a point where the staple can move from one helix to the other without significant bending and retaining the helicoid shape. In B-DNA a complete turn happens every 10.5 base pairs, but multiples of this value can be used to retain a round number of base pairs (for example every 21 for two turns). The crossover positions are where the staples will link the two helices together, holding them in place and giving robustness to the structure, which will then be formed of helices bundled together in a lattice. Depending on which crossovers are used to form it, both square and hexagonal lattices can be implemented. One of the most important advantages of this technique is its high precision at a nanometric level, as the base to base distance in DNA is  $\sim 3.4 \text{ \AA}$ , allowing to create features with a resolution of a few nanometers in structures that are limited in size only by the scaffold length, usually a few kilobases long (7249 for one of the most used, the DNA extracted from the M13mp18, a phage vector).

One of the first pieces of software developed for the design of DNA origami is *cadnano*<sup>6</sup>, available for free and still today probably the most used in research laboratories. It allows the user to draw the desired structure by bending and folding the scaffold strand, before adding the staples to fix the design. The final result of the automated design is to suggest staples sequences, according to the scaffold DNA used, that can be artificially synthesized by companies, such as Thermo Fischer or IDT.

Having the scaffold strand and the staples, the researcher can mix them and perform an annealing step in a thermocycler, to obtain the final DNA origami solution. In addition

to the DNA strands, a buffer is used to keep the pH constant (1x TAE) with the addition of 12.5 mM  $\text{MgCl}_2$  that ionizes to  $\text{Mg}^{++}$  to stabilize the DNA duplex. A few words should be said about the annealing process: the binding of complementary strands is a process that is energetically favourable, but few hundreds of staples have to all find their way onto the scaffold and this process has to happen for all the molecules in the tube. To facilitate this, staples are always used in excess, with a molarity 10-20 times higher with respect to the scaffold. The system then needs enough kinetic energy for the molecules to move, thus creating binding occasions when they get in contact with each other; this energy is given to the system thermally, bringing the solution to 90 °C and then slowly cooling it to 20 °C, one degree per minute. Certainly the final tube will contain an excess of staples and, depending on its final application, should be purified, removing the unbound staples and keeping pure DNA origami.

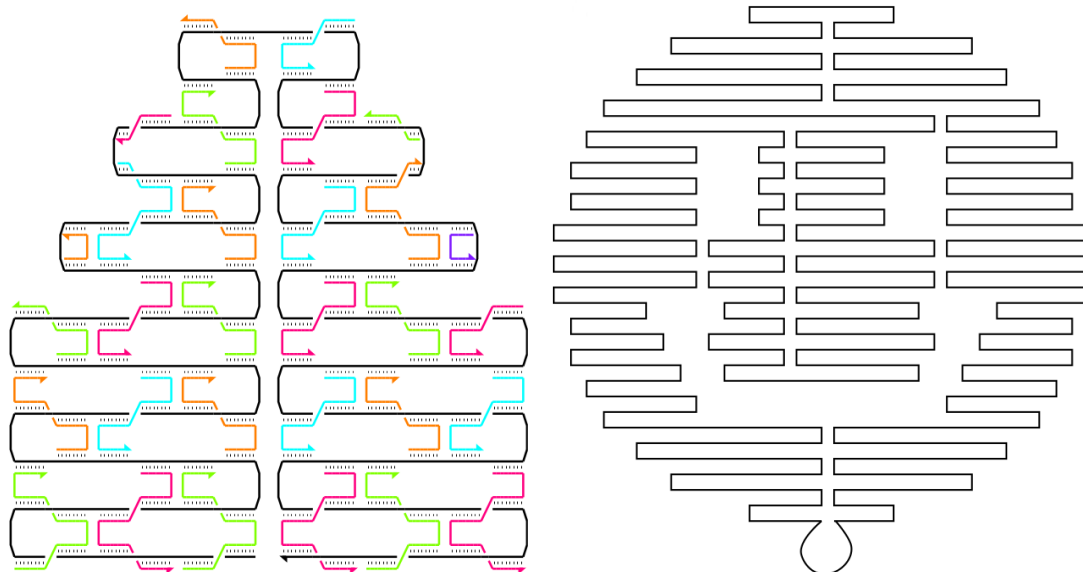


**Figure 1.3** – DNA origami lattice showing only the scaffold. Reprinted by permission from Springer Nature: Nature [5], copyright 2006. **Figure 1.4** – DNA origami design of a smiling scaffold and staples on the final design. Reprinted by permission from Springer Nature: Nature [5], copyright 2006.

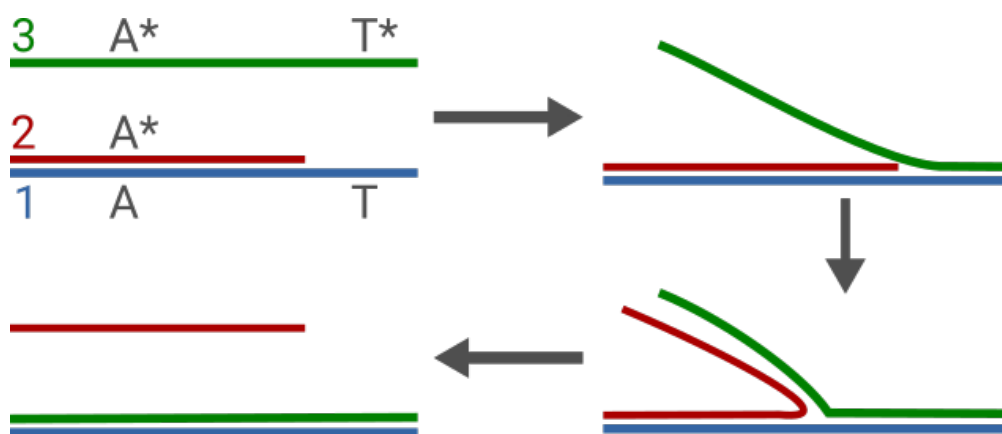


**Figure 1.5** – DNA strand displacement process where strand 1 and 2 are hybridized along sequence A, strand 3 binds to toehold T and proceeds to displace strand 2, removing it and forming a double helix with strand 1. Stars represent complementary sequence. 5' and 3' ends are not shown, but strand 1 is antiparallel to strand 2 and 3 in order to be able to hybridize (reverse complement).

### 1.1.2 DNA Strand Displacement

DNA strand displacement is a technique that can be used to dehybridize a DNA double helix and rehybridize one of its strand to a third invader strand. Figure 1.5 shows the mechanism of the reaction. Strands 1 and 2 are hybridized along sequence A, but strand 1 also has a single stranded, unhybridized short sequence T, called toehold. Strand 3 is perfectly complementary to strand 1 and, when it is added to the test tube, it will bind to Y initially and then will displace strand 2, forming a double helix that is energetically favorable with respect to the starting system. As the reaction starts from the toehold sequence, it is also called toehold mediated strand displacement.

This method has been widely used to design logic gates that can perform digital operations on DNA strands<sup>7</sup>, but it can also be used in DNA assemblies with structural functions. For example a two piece origami could be divided via strand displacement or a box could be opened when the right key strand is added<sup>8</sup>.

## 1.2 Electrochemical Transduction

Expand: Nernst  
and theory of redox

Electrochemistry is the discipline that lies at the intersection between chemistry and electrical effects, studying the transfer of electrons in chemical reactions, particularly in

oxidation-reduction reactions (redox). This process can be formally written as:



The reduction process goes from left to right and consists in the gain of  $n$  electrons by the species  $O$ , leading to the reduced species  $R$ . By contrast, the oxidation process is the loss of  $n$  electrons from  $R$  to  $O$ .

This reaction happens between two electrodes which are immersed in a conductive solution (electrolyte) and the circuit is closed with a voltage source. The aim of this might be to start a reaction that might not be possible or very difficult without electrical work, or it could be, as in this work, to study the properties of such process. While the first case is interested only in applying the necessary voltage, the second case requires to measure the response of the system and record the output current. In every experiment, a voltage will be the input and a current will be the output, however the opposite is also possible, while less common.

To understand a redox reaction, the whole system, electrodes included, should be thought of as an electrical circuit. When a voltage generator is inserted, an electron flow is expected, if the circuit can be closed, and this electron flow will be constant in each part of the circuit. What happens inside the electrochemical cell should then be represented by the same conditions. Specifically one species will be oxidized and the other one reduced, thus creating a flow of electrons in solution from one to the other and closing the circuit. When this happens, the current is higher and the effective resistance of the system decreases, while under different conditions the only current measured comes from the small conductivity of the electrolyte solution itself.

The transfer of electrons is most often non spontaneous, as the electrons do not have enough energy to leave the system, so that a voltage has to be applied in order to increase it and make the reaction favourable. This happens for both sides and reactions in the cell, the one losing electrons and the one gaining them, so that the required potential for each of the two processes is difficult to extract, as they are codependent. Special electrodes that can maintain a fixed potential have been developed (“reference electrodes”), so that the reaction potential of other reactions can be measured against them, without having to worry for a second reaction.

In order to describe these phenomena quantitatively, it is useful to consider them at ther-

modynamic equilibrium, that is to say that the process will reverse direction when the driving forces are reversed infinitesimally<sup>9</sup>. While this is not possible unless the driving forces themselves are infinitesimal at every time step, a system in which they are small and slow enough can be practically considered reversible, so that one can study it out of equilibrium. In this regime, the electrode potential can be described by the Nernst equation:

$$E = E^0 + \frac{RT}{nF} \ln \frac{C_O}{C_R}$$

which shows the relation between the potential seen at the electrodes  $E$  and the concentration of oxidized and reduced species ( $C_O$  and  $C_R$ ).  $E^0$  is the reaction potential when the concentrations are equal and is called standard reaction potential, while  $R$  is the gas constant,  $T$  the temperature,  $F$  the Faraday constant (charge per mole of electrons) and  $n$  is the number of electrons exchanged in every single reaction event. This relation describes the trend of the electrode potential while the redox transforms one species into the other, until the former has been depleted, ending the reaction. While this explains very well the voltage decay in a battery, in our experiments the two concentrations are continually replenished by reversing the voltage potential until all the molecules have been oxidized or reduced again. In this case, one can reverse the equation and see how, while a voltage is scanned, the concentration changes, which can be seen as how many molecules are reacting at each potential and translated as the number of electrons exchanged (current) in every measurement.

### 1.2.1 Measurement Setup

In scientific experiments the outside setup is a potentiostat, an instrument connected between the electrodes that can generate voltage waves and then measure the current response of the system. To do so efficiently, a so-called "three electrode setup" is required. The first one is the working electrode, that is the functionalized sample to be measured, one of the two ends between which the voltage is imposed and the current measured. Then the counter-electrode supplies or receives the electrons for the reaction and it is the second node where the current is measured. It should be able to react almost instantly so that the flux of charge can accommodate the reaction at the other end, without limiting it and for this reason it often has a much larger surface. To be

more precise, a half-reaction occurs at the working electrode and a half-reaction occurs at the counter electrode: one balances and supports the other one and the cell would not work with only one of them. In most cases, the redox of interest occurs at the working electrode only, thus it is convenient to choose counter electrodes with great availability of electrons and fast transfer, so that this is not the limiting factor of the system. The third electrode is called reference electrode and it is the second end where the voltage is applied. Fixing a precise potential difference is critical, but the potential of any electrode is set by the reaction happening on it. Thus, any reaction would change the potential of the electrodes separately and this is for us an unknown parameter, as we can only control the voltage (potential difference). This is why the reference electrode must be chosen so that is almost inactive in measurement conditions. Their inertness means that their potential hardly changes, thus the only potential that can change is the one on the working electrode, that can be then seen as a voltage change. On the other hand, their inactivity also means that there is no exchange of electron, so that they could not sustain a current from the working electrode, thus the need for the counter electrode to balance the half reaction.

The standard hydrogen electrode (SHE) is the most common reference electrode against which reaction potentials are reported, however it is rarely used in practice and others are favored over it depending on the reactivity of the system to the elements in th. The choice here has been to use a silver chloride electrode where the reaction takes place between the silver wire and the silver chloride salt. The source of chloride ions is the *KCl* solution in which the silver wire is placed, however a membrane prevents any leak into the electrochemical cell itself, so that the electrolyte is not contaminated. Figure 1.6 shows the physical implementation of such a design, as used in the following experiments. The cell, as shown in Figure 1.7, comprises the experimental setup external to the potentiostat, where the reactions occur. On the bottom the working electrode is the functionalized gold sample, in contact with the electrolyte solution. Above it, always in the solution, are placed the two other connections: reference and counter electrode. The sample itself is held in place by two screws that push it against the teflon cell, preventing any spill of electrolyte. To be able to do this, the gold substrate requires a silicone gasket (Figure 1.8) in which the reaction will actually happen and that will hermetically seal the system. Thus, any sample preparation starts by gluing the gasket and all the

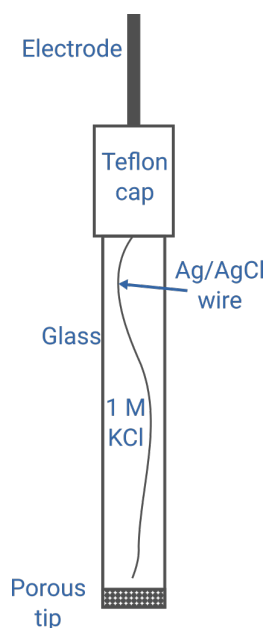


**Figure 1.6** – Scheme of an Ag/AgCl reference electrode.

deposition steps are performed inside it, not on the entire chip surface. Moreover, to close the electrical circuit, a low resistivity copper tape is attached on the gold and then clasped by the potentiostat connectors.

The following paragraph describes some of undesired reactions and noise sources in electrochemical measurements. The rest of the chapter is dedicated to the description of the most common techniques for the study of electrochemical systems, at least the ones used in this work. The aim is to describe the principles and hint at how each of them could be used for different measurements that will be treated later on.

### 1.2.2 Nonfaradaic and faradaic disturbances

The reaction of interest is never the only process happening inside an electrochemical cell or the surrounding setup, so that the measured traces must be interpreted in light of a series of different undesired phenomena. However careful study and sample preparation allow to minimize these disturbances and facilitate the post-processing and data analysis. Faradaic is a term that describes electrical processes governed by Faraday's law, that describes electrochemical reactions where the current is quantitatively related to the reaction happening, such as those of interest in each measurement. On the other side, nonfaradaic processes do not have a direct effect on the composition of electrodes



**Figure 1.7** – Electrochemical cell mounted with the gold working electrode (on the bot-

tom, visible through the hole), the reference electrode (larger on top) and the counter electrode (the silver wire on the bottom right). The electrolyte solution is here 1x PBS and fills the entire cell.



**Figure 1.8** – Gold sample with silicone gasket and copper tape.

or solution and might instead happen as a result of these changes. One of the most common and easy to understand is the capacitance of the electrode, seen at the interface between the electrode and solution, where charge is accumulated on each side. This is called electrical double layer and its disturbance can be minimized by applying a voltage step and then waiting for the capacitance to fully load, before proceeding with the experiment. However some such effects are still sometimes visible in the final trace and can be noticed by a rapid charge at the very beginning of the measurement.

The most important disturbance on gold electrodes is however due to a faradaic phenomenon that happens in solution and easily overpowers the signal from the redox indicators. It is due to the reduction of free oxygen in solution that can result in water (with or without a peroxide intermediate step<sup>10</sup>). If the electrode has not been passivated, this background completely covers any fine measurement from negative voltages up to more than 1 V (against Ag/AgCl). However, if the electrode has been passivated with a self-assembled monolayer that covers the surface and renders it inaccessible, a large voltage window is available without significant disturbance. Even in this case, moving

towards more negative voltages (0.5-0.6 V vs Ag/AgCl), the effect of the oxygen current rises to several microamperes. Another solution to the problem is performing all the experiments in absence of oxygen, by using a N<sub>2</sub> atmosphere and degassing the electrolyte solution. While this leads to improved results, it is very difficult to completely free the environment from oxygen and very negative voltages should be avoided.

### 1.2.3 Cyclic Voltammetry

Applying a potential sweep to an electrochemical cell is one of the easiest and most straight-forward techniques to study a redox process. In cyclic voltammetry the sweep is applied linearly between two voltages in both directions for several cycles and the resulting current is measured and plotted.

To clearly show the working principles of this method, it can be useful to apply it

improve quality of image

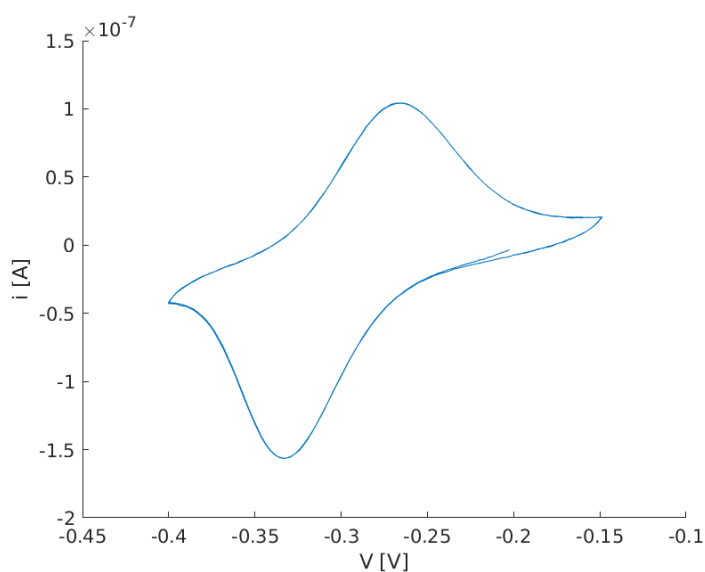


**Figure 1.9** – Cyclic voltammogram of methylene blue on a double-stranded EDNA molecule in 1x PBS .

theoretically to a common electrical component, for example a resistor. Applying a linearly increasing voltage between its ends would result in a linearly increasing current, plotting a segment with slope equal to its resistance. When the sweep direction is inverted, the segment ends and the plot would move back along the same line and then this is repeated for as many times as the measurement cycles. In a real system, how-

ever undesired components would always be present and should be taken into account. For example parasitic capacitances would have to be loaded in both directions and this would introduce hysteresis cycles where some of the current is not actually due to the resistance, but to the charging effect. These processes are also present in electrochemical measurements due to the same reasons as well as other undesired faradaic phenomena (as those described before in Section 1.2).

Figure 1.9 shows an example of a generic measurement of methylene blue redox between  $-0.15$  V and  $-0.4$  V. The cell is first brought to a starting voltage of  $-0.2$  V for a few seconds in order to charge any parasitic capacitance and reach equilibrium. Then the sweep starts towards negative voltages, in the anodic direction at a scan rate set by the user, in this case  $-0.01$  V/s. Approaching the standard potential of the species, the molecules start to react and accept electrons, creating a negative current between the gold electrode and the counter electrode. The current reaches a peak at a certain voltage  $A$  and then start so decrease until the switching voltage is reached.

Then the direction of the sweep is reversed in the cathodic direction ( $0.01$  V/s) and a new peak current is reached when the methylene blue molecules donate electrons, until the switching potential is reached at  $-0.15$  V. The cycle is repeated again to remove some of the non-faradaic currents. Figure 1.9 clearly shows that the peaks do not have a zero flat baseline, but instead rise on top of the background currents, differently from what expected in the ideal case. The background is not due to the redox indicators in solution, but to other undesired factors, such as oxygen currents from the gold substrate, that form the baseline signal and act as noise in the measurement. Moreover, the whole plot is tilted by some degrees and this inherently indicates a resistive behaviour, due to the resistance of both the solution and the electrical contacts. These factors have to be taken into account when analyzing the measurements and subsequent sections will be dedicated to this.

An important parameter in cyclic voltammograms is the scan rate, which is how many volts are being scanned each second, this of course translates in a faster or slower measurement, but has important effects on the system itself. A slower sweep keeps the system more reversible while it is slowly moved from one equilibrium point to another, giving it time to settle in the new state at each step. On the other hand a faster measurement, while still being linear, does not allow this time for the molecules to adapt and react.

The very definition of thermodynamic and chemical reversibility implies that reversing the process, in this case the sweep direction, would reverse the reaction following the same equilibrium states<sup>9</sup>. While thermodynamic reversibility requires infinite time, a chemically reversible system scanned over a long enough time can approach it, with one limitation. To go through the same states once the scan direction is reversed means that if the peak in the anodic sweep is found at voltage X, it should also be found at the same voltage X in the cathodic direction, as reversing the reaction right at that point should position us in the same state (the one of maximum electron exchange). However cyclic voltammograms have a theoretical limitation of peak separation equal to  $59 \text{ mV}/n$  (at 25 °C and where  $n$  is the number of electron per reaction event). This is due to the kinetics of electron extraction which still require some energy, but it is only valid for phenomena happening in solution, it can be overcome for surface reactions, such as most of what will be treated hereon.

We can force this to happen with redox indicators positioned directly on surface. By tuning the scan rate, we can have peaks that have virtually zero separation and then, accelerating the sweep, we can start to see separation, meaning that the system has reached a reversibility limit. Instead of changing the scan rate and forcing this behaviour, it is more interesting to keep its value fixed, but analyze how different systems respond to it. A good example of this will be shown in Figure 1.19, where the same DNA sensor is modified by an analyte, drastically changing its kinetics.

#### 1.2.4 Alternating Current Voltammetry

Pulse voltammetry is the general name for any method where the potential is changed as a step, instead of a linear approximation. In the case of alternating current (AC) voltammetry, a DC signal is applied and stepped up slowly with time from one end to the other of a predefined range. On top of this is applied a significant (around 20-50 mV) AC signal<sup>a</sup>, hence the name AC voltammetry. This means that the system is moved to different equilibrium states (the potential steps) slowly, so that it can adapt to them, but after this the AC signal disrupts the equilibrium and forces the reaction on a less reversible path.

---

<sup>a</sup>AC is used here, as common convention, also to indicate alternate voltage.

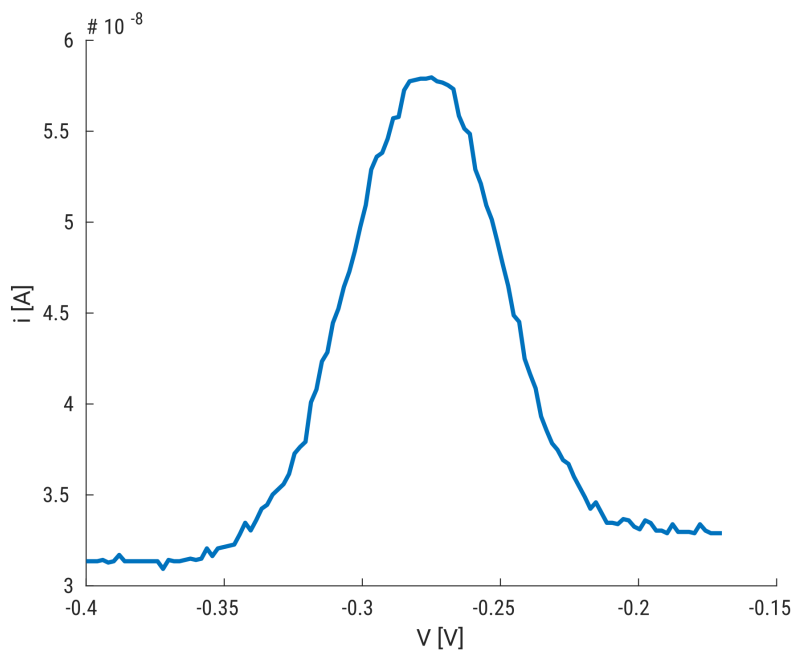


**Figure 1.10** – Example of an AC voltammogram performed on a sample with methylene blue, visible in the peak centered around its reaction potential of -0.28 V.

The scan is not cyclic, as this would provide no advantage, and the measurement is performed only in one chosen direction, which also should not affect the experiment. Thanks to the use of alternate currents, the information about the phase is available, which can be used to determine real and imaginary parts of the impedance, thus giving broader information about capacitances and inductances in the system.

The main resulting plot, however, is the magnitude of the AC component of the current response per each potential step. An example of this for a methylene blue experiment is shown in Figure 1.10

### 1.2.5 Square Wave Voltammetry

Square wave voltammetry (SWV) is a pulse voltammetry technique that uses two superposed voltage staircases as input. Figure 1.11 shows this signal: a slowly increasing step is added onto a non-return to zero pulse with a much higher amplitude and a period equal to half the step. The current is measured at the end of each half step, positive and negative and the two are subtracted resulting in a difference current over voltage plot, where the voltage is indicated by the slower staircase.

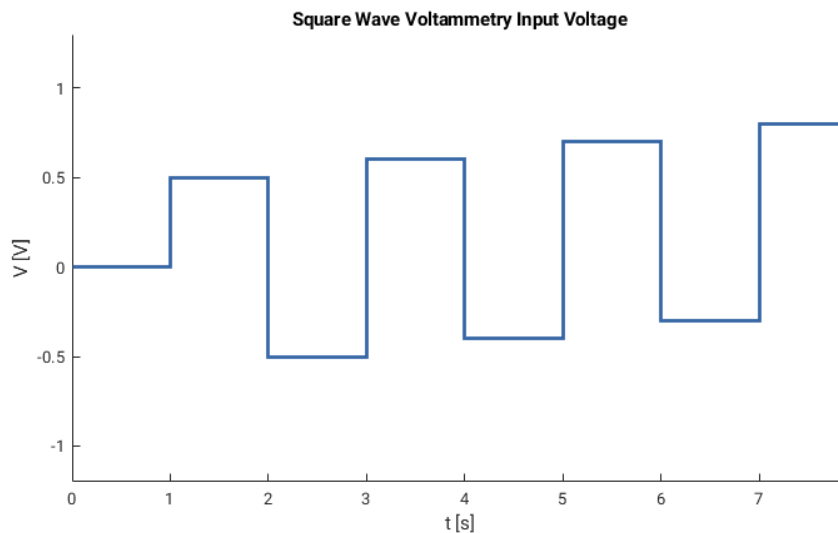


**Figure 1.11** – Input voltage ramp in a square wave voltammogram.

A peak is read on the output and its shape and height are related also to the frequency of the applied pulse signal. It is then possible to perform a sweep of different square wave voltammograms at different frequencies and compare the response of the system. This kind of analysis yields information on the optimal conditions to interrogate the cell, as, the higher the peak height, the more the contrast between signal and background noise. To show this, even if the sensor working principle has not been introduced yet, Figure 1.12 shows two plots for the system at rest and after it has been saturated by the analyte molecules. This peculiar kind of curve show the height of the peak current measured in square wave voltammetry for a number of different frequencies of the pulse signal. It is evident how at some frequencies, for example  $\sim 10$  Hz, there is no real difference between the two cases and applying that input would not allow to measure any analyte concentration. However, one can also see that at  $\sim 25$  Hz, the separation between the two responses is very high, thus such input could be applied to characterize the sensor.

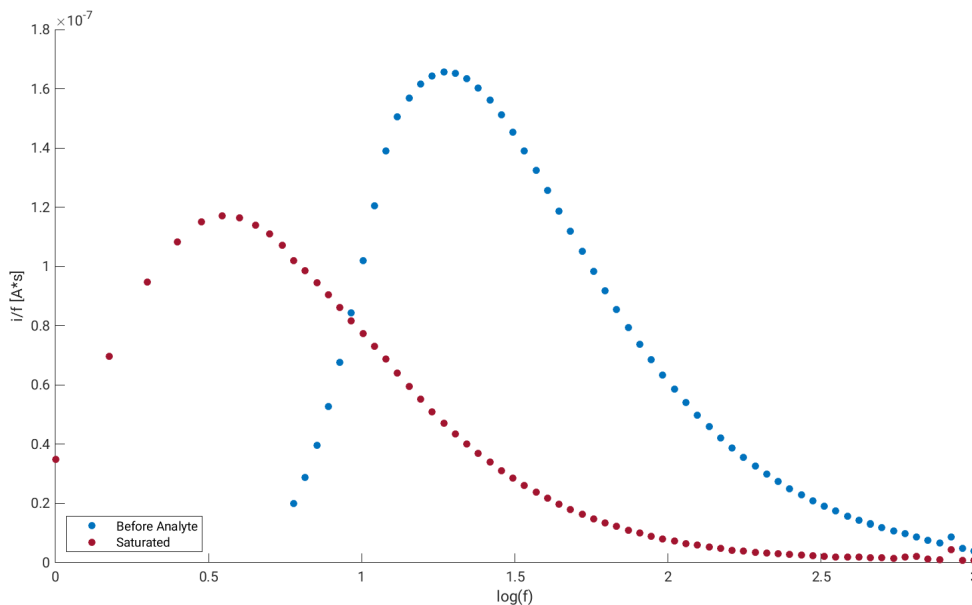


**Figure 1.12** – Plot of a SWV sweep on frequency for two systems, one at rest and one after saturation with the analyte molecule. The current is normalized for the frequency (Lovrić plot, explained in detail later).

### 1.2.6 Impedance Spectroscopy

Impedance spectroscopy (IS) is one of several techniques that look at the small signal response of the electrochemical cell and study its impedance, modelling it as a fitted discrete circuit. Its name also implies that this is done at different frequencies, by applying a DC signal, so that the electrode potential is close to the standard reaction potential, and superposing a small AC signal on top of it. The measurements is swept across a large range of AC frequencies, namely from 10 kHz to 0.01 Hz in our studies, and the values of real and imaginary impedance are reported on a Nyquist plot. The difference with AC voltammetry described before is that here the sweep is done over frequencies, while, in the other case, it is the DC voltage offset that is swept. Then, while AC voltammetry looks directly at the current response, impedance spectroscopy further process it to extract the impedance values.

The most common ideal circuit used to fit these measurements is a Randles circuit, shown in Figure 1.13.

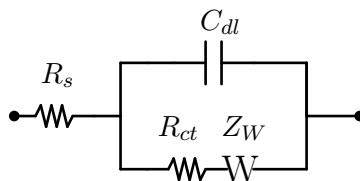


**Figure 1.13** – Randles equivalent circuit for electrochemical interfaces.

The two external nodes represent on one side the working electrode, on the other side the reference and counter electrode, for voltage and for current respectively. The first element  $R_s$  is the solution resistance, that limits the passage of current, but does not have any role in the electrochemical reaction. This instead is modelled by the other three elements, a parallel between a capacitance and a series of a resistance and a constant phase element called Warburg element.  $C_{dl}$  is the capacitance of the electrical double layer due to the potential drop at the interface between solid electrode and liquid electrolyte, forcing a charge accumulation seen here in its dielectric effect.  $R_{ct}$  models the charge transfer resistance due to the limiting factors of the reaction, for example electron transfer or other preliminary reactions, while  $Z_W$  represents the mass transfer limitation and tends to disappear at higher frequencies, where there is no time for physical diffusion to interfere with the current.

The general shape of a Nyquist plot measured from an IS experiment is shown in Figure 1.14. The direction of increasing frequencies is from right to left. While the theory is not shown here (see [9]), the shape of the curves directly translates to  $C_{dl}$ ,  $R_{ct}$  and  $R_s$ , while  $Z_W$  can be calculated if needed. The intersection on the x axis represents the value of  $R_s$  (a purely resistive element has only a real component to it), while the diameter of the circle drawn on the same arc is  $R_{ct}$ .  $C_{dl}$  can be found by looking at the frequency that corresponds to the center of the circle drawn on the arc and writing it as  $\omega = 1/R_{ct}C_{dl}$ . The Warburg element is represented as a line with slope equal to one that, at lower frequencies, can prevail on the resistive components.

There are different electrochemical systems where the balance between the two components might be severely shifted towards one or another, leaving with plots that only show a line, for reactions dominated by mass transfer, or an almost perfect semicircle, where diffusion is not at play.

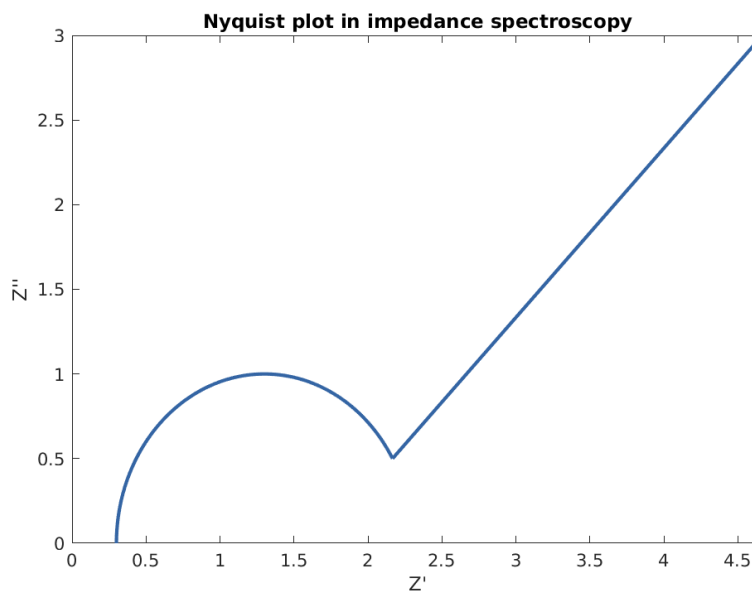


**Figure 1.14** – Resulting Nyquist plot in a typical impedance spectroscopy setup.

Finally, it is worth noting that one of the parameters of interest in these studies is the electron transfer rate, the frequency with which the electrons are exchanged in the reaction. This can be extracted starting from the resistive components of the circuit, but, if the Warburg element is dominant, no information on these can be obtained. Instead of simply disregarding the technique in these cases, this gives a strong indication that any such experiment, as it has been designed, will never be able to provide valuable electron transfer rate values, since the system is limited by mass diffusion and not by the speed of the reaction itself.

### 1.3 Biological Sensors

Biological sensing is a broad and ever expanding field, thanks to the wide variety of analytes, from DNA and RNA to proteins and enzymes, that in turn can be expressions and indicators of processes or diseases to be measured. Not only the number of targets is very high, but their reactivity is also an important factor, with several techniques that have been developed to link them to different molecules, from fluorophores to magnetic beads, so that transduction can be performed with any choice of readout methods.

It would be overwhelming and beyond our scope to describe extensively different tech-

niques, so this section is organized with a choice of few examples that will be functional to the work presented later. The enzyme-linked immunosorbent assay (ELISA) is one of the most popular and used methods, one that is a direct competitor and point of reference, not only for the DNA origami sensor designed here, but for any new entry in this field.

EDNA is less well-known and does not yet have viable commercial applications, but it was the starting system from which our project stemmed and they still share some of the principles. Thanks to its simplicity, it is also a very robust and reproducible tool that we use to train our electrochemistry abilities and perform some of the preliminary studies of Chapter 2.

Finally we describe the concept of the DNA origami sensor, highlighting its advantages and possible challenges.

### 1.3.1 Enzyme-linked Immunosorbent Assay (ELISA)

### 1.3.2 EDNA

EDNA is a detection system that has been developed by Plaxco's group at UCSB and has been used in the last fifteen years to detect DNA fragments and small proteins. The principle behind it exploits one or more surface bound DNA probes that undergo a change in structure upon the binding of the target analyte. These probes are labeled with redox indicators and the conformational change brings these molecules closer or further from the surface to which the DNA probes are bound, a gold electrode. In the proximity of the surface, when sufficient voltage is applied to the system, the redox indicators can be reduced and will release electrons in the process, while, at higher distances, the process is inhibited or slowed down, requiring more energy. The electrons are collected on the gold electrode and will produce a current read by the potentiostat, the final readout mechanism. The change in conformation means a higher or lower electron transfer when the target is present or absent, allowing to see a change in current when the measurement is performed.

Figure 1.15 visually explains the working principle of the system in its first iteration<sup>11</sup>. A single DNA strand is partially self-complementary and forms a dumbbell hairpin

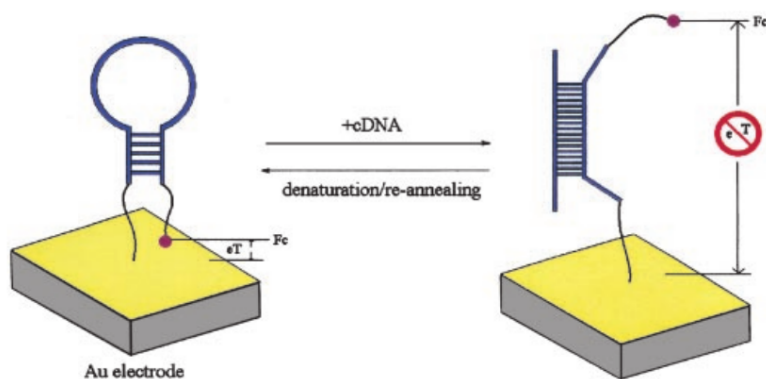


**Figure 1.15** – EDNA system for DNA fragments detection from [11], without target analyte on the left and after invasion on the right. Copyright 2003 National Academy of Sciences.

structure, with the two extremities hybridized, while the middle part, that is not self-complementary, forms a hairpin and remains single stranded. On one end the DNA strand has a thiol group that binds it to the gold surface, on the other end a ferrocene molecule is kept close to the surface by the formation of the hairpin.

Ferrocene is a redox reactive molecule (with half-reaction  $Fc^+/Fc$ ) and its proximity to the surface allows for easy electron tunneling with fast kinetics (the rate with which electrons are exchanged).

The target analyte is the DNA strand that binds to the hairpin region left exposed, opening the two ends and bringing them apart. These two states are thermodynamically competitive and must be studied so that the favorable equilibrium state is the new one with the analyte hybridized, so that its presence is actually detected. The ferrocene molecule is now further from the surface than in the previous configuration and the rate of electron transfer slows down.

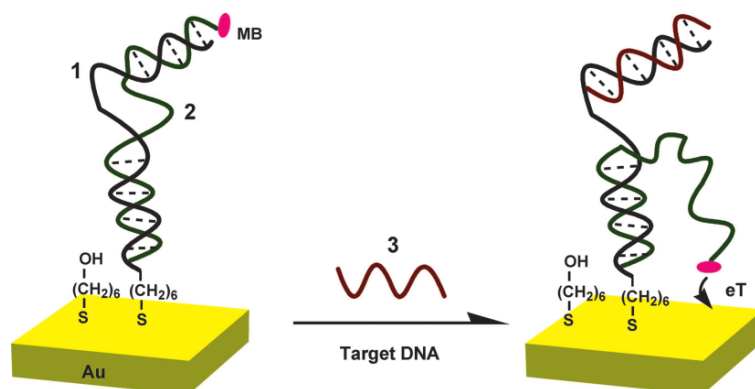


**Figure 1.16** – EDNA system for DNA fragments detection from [12] using methylene blue as a redox indicator. Copyright 2006 National Academy of Sciences.

A more advanced system is shown in Figure 1.16: ferrocene has been substituted by methylene blue (MB), another redox indicator that has the advantage of being more stable<sup>13</sup>, leading to better sensitivity. Furthermore, the sensor is now “signal-on” which means that adding the target analyte increases the current response of the signal (by bringing the MB closer to the surface), instead of decreasing it as done previously. This allows for greater contrast (in a signal-off design the maximum change is 100% of the starting signal) and eliminates the presence of false positive due to the degradation of the system<sup>14</sup>.

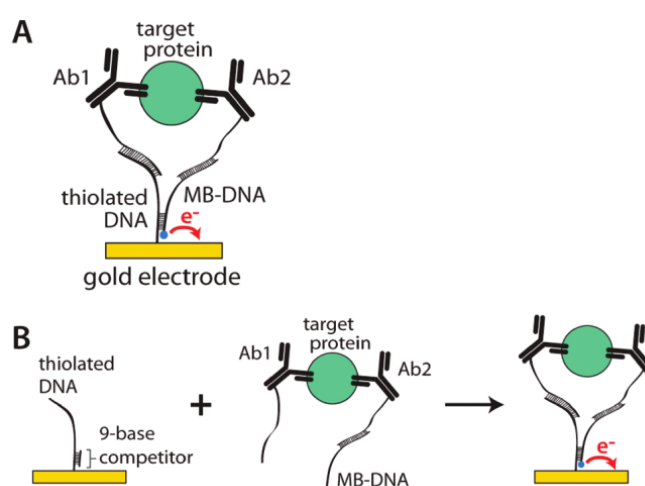


**Figure 1.17** – EDNA system for protein detection. A) Final system with analyte B) Assembly of the system. Reprinted with permission from [15]. Copyright 2012 American Chemical Society.

Going further, Figure 1.17 describes a modification<sup>15</sup> of the system in order to accommodate a protein binding complex formed by two aptamers and two antibodies (Ab1 and Ab2). The design is different due to the larger size that requires a new way to bring MB molecules close to the surface (by placing them on another oligonucleotide) while maintaining the flexibility of the assembly. Notably the detection limit of this system is in the range of femtomoles, which can compete with ELISA kits for insulin detection<sup>15</sup>. A further advancement was the implementation of an EDNA system in vivo for drug measurement<sup>16</sup>, which requires a closed system that does not have any free molecules that can enter the organism on which the test is performed.

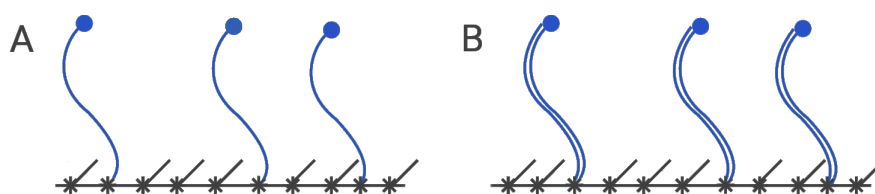


**Figure 1.18** – EDNA design used in this work. A) Single stranded EDNA without analyte. B) Double stranded EDNA after target invasion.

The system used for the preliminary experiments and measurements is again different from the previous ones and it lends itself to such uses thanks to the extreme simplicity of its design. A scheme is shown in Figure 1.18: a single stranded DNA has a MB molecule on the unbound end and is free to bend bringing it close to the surface. The addition of the complementary strand (analyte) hybridizes it to form a double stranded DNA, stiffer and less flexible. MB molecules can still be brought close to the surface enough for electron tunneling to happen, but the energy required to move them is very different and this is shown in the kinetics of the system.

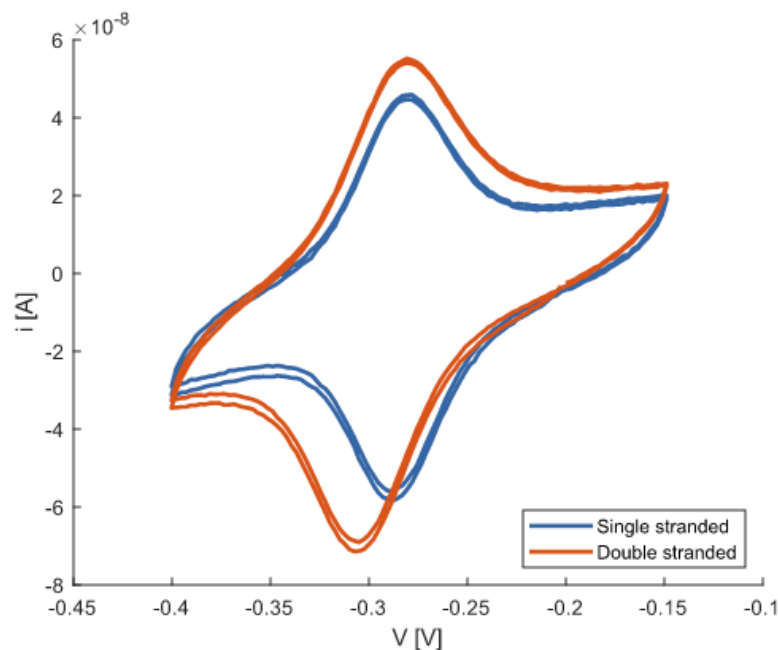


**Figure 1.19** – Cyclic voltammograms of the EDNA system of Figure 1.18 before and after adding complementary target strands

1.19 shows the superposition of the two plots for uncomplemented and complemented EDNA. If the kinetics of methylene blue on EDNA make for a reversible process at the chosen scan rate (0.01 V/s), one can see how this changes by changing the system geometry, even only by hybridizing these strands with their complementary sequence. The single stranded EDNA has almost no peak separation, meaning that the reaction is highly electrochemically reversible and thus that the electron transfer rate is very high. Then, when EDNA has been complemented by the analyte, the reaction moves towards irreversibility, with the two peaks starting to split. It is evident that double stranded EDNA has a noticeable peak separation (around 0.03 mV) which indicates a less reversible system due to the fact that the DNA double helix is stiffer and prevents methylene blue molecules to reach the surface, thus requiring higher energies to transfer electrons. The detection of the analyte is performed through measurement techniques that are heavily influenced by the transfer rate, such as square wave voltammetry, as will be explained in Section 2.4.

For brevity, further references to EDNA will always refer to this specific system configuration, unless otherwise stated.

### 1.3.3 DNA Origami Sensor Concept

The DNA origami technology described in Paragraph 1.1.1 allows to fabricate two and three dimensional structures that are not capable of movement or change in their shape, as structural integrity is usually the first requirement. However different methods can alter this and lead to DNA origami that feature movable parts with control on their states.

Omitting some of the staples, for example, locally weakens the rigidity and allows the origami to bend along that missing seam. In the same way the missing staples could be added to the sample after the first annealing of the origami, reforming double stranded DNA in every point and increasing the stress resistance, thus possibly recreating the desired original shape. One prime example of such behaviour was demonstrated by creating a 3D DNA nanobox with a lid controllable with a "DNA key"<sup>8</sup>, as in Figure 1.20. Here the flexibility of the lid is guaranteed by hinges made of single stranded scaffold linker (absence of staples) and the box itself is held close by two sticky ends. A sticky end is a single stranded tail (A) of DNA protruding from the structure that can bind to its reverse complement (A\*) located in another part of the structure.

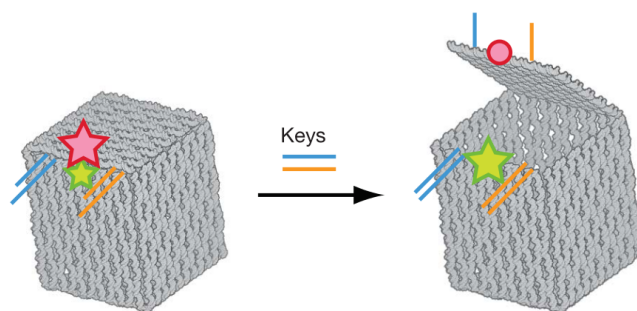


**Figure 1.20** – DNA box with a controllable lid, the two sticky ends (orange and blue) can be opened via toehold mediated displacement by the two keys. The stars and circle represent a fluorophore and its quencher. Adapted by permission from Springer Nature: Nature [8], copyright 2009.

One of the strands in each sticky end has a toehold overhang, so that the lock can be displaced using toehold mediated strand displacement (Paragraph 1.1.2). Once the keys have hybridized the lock, the other sticky end is free to be released and the lid can be opened, for example by thermal energy. This is confirmed by using a fluorophore located

on the edge of the box that starts emitting once its quencher, on the lid, is moved away from it. Such a structure could be applied for targeted drug delivery or to localize a reaction in a confined environment<sup>17</sup>.

The DNA origami sensor in this design exploits a similar technique in order to have two stable states, one in the absence of analyte molecules and one in their presence. The two main aims are to be able to bring the redox indicator molecules far enough from the surface that virtually no electron transfer can happen and to accommodate large sensing complexes, such as the ensemble of antibodies needed for some proteins detection. Having the MB molecules (or other indicators) far from the electrode is difficult for EDNA sensors as it would require long DNA strands, significantly more than the 40-60 bp ( $\sim 14$ -20 nm) usually considered as limit for the synthesis technology. The same limitations requires the analyte to be small enough to still be able to bring the MB close enough to the surface to have a significant signal change.

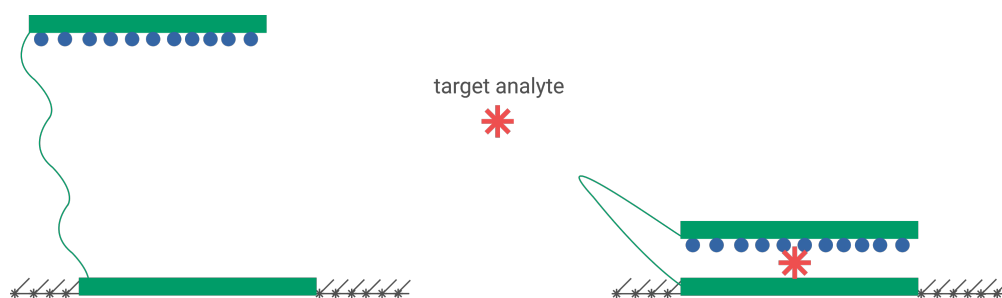


**Figure 1.21** – DNA Origami sensor design. On the left open configuration in the absence of analyte molecules. On the right closed structure after the binding with the analyte molecule.

The design for the origami is shown in Figure 1.21: it is divided in two parts, one that is bound to the electrode on the bottom and the other one that is free to float in solution, with a long ( $> 1$  kbp) linker holding them together as a single molecule. The top lid is loaded with methylene blue molecules and the presence of the analyte brings it down, closing the structure. This can happen with two antibodies, one on each part, for proteins or with partially complementary DNA strands on each part for DNA detection. This sensor has been named venus flytrap as its working principles are heavily inspired by the carnivorous plant, that similarly closes its mouths when insects stimulate them. While the general design is fixed here, most of its parts are not set and several solutions

---

are being tested in the lab. An important challenge lies in designing a two part origami with current available scaffolds of limited length: it would mean that the two structures and the linker all have to be folded on the same few kilobases long scaffold, thus making each of them quite small. In another solution, two different origami could be folded using the same scaffold sequence separately, so as to avoid the staples from one hybridizing to the other, and then linked together with a third linker strand once they are fully formed. Or again, once they are commercially available, different orthogonal scaffolds could be used to obtain the same result in one test tube. One of the reasons why the two parts need to have a large surface area is the detection of large molecules, such as some proteins: if the upper structure can be folded in a dome-like shape, the antigen-antibody complex can sit in the middle, while the MB molecules on the edge can still reach the surface. The freedom to design different structures and curvatures come at the price of needing more bases for the same area.



# Preliminary Electrochemical Measurements

maybe short intro

## 2.1 Stepwise Fabrication Control

The fabrication of the final electrode is a lengthy process that requires several steps. The gold surface, after being diced, has to be cleaned, then the DNA is deposited and finally the passivation monolayer assembles on the surface. This last step is the one that effectively makes methylene blue molecules measurable, by removing the much higher background currents on the gold. The fabrication process just described applies generally to EDNA experiments as the ones described in this chapter, some modifications might be needed for DNA origami.

Each of these steps effects the surface of the electrode, thus, from an electrical standpoint, it changes its behavior as a capacitor and a resistor, which can be easily tested with impedance spectroscopy. The idea is to have redox indicators dispersed in solution and, once the cell is brought to the reaction potential, study their response, how easily they can reach the surface, how easily they can be reduced. It is most often done by using ferrocyanide  $[\text{Fe}(\text{CN})_6]^{3-}/[\text{Fe}(\text{CN})_6]^{4-}$  in solution and fitting a Randles circuit to the impedance seen by this reaction at different frequencies. However any redox indicator can substitute it, provided that the kinetics of its reaction are not limiting. For the first test we decided to proceed with methylene blue which was readily available in the lab. After each fabrication step, the electrode is measured in a 4  $\mu\text{M}$  MB in 1x PBS solution, the impedance is measured between 10 kHz and 0.01 Hz and the Nyquist plot is fitted against the Randles circuit elements. When a monolayer is formed on surface, it will change the capacitance seen by the circuit, with its dielectric constant, but it will also create a barrier for the redox indicator in solution which will not be able to easily reach

the electrode and thus the resistance will also increase.

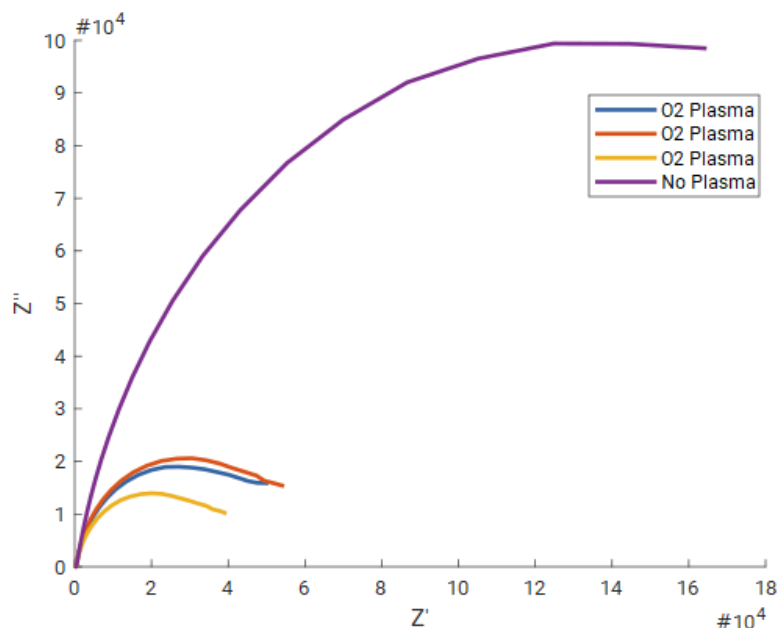


**Figure 2.1** – Impedance spectroscopy measurement of different gold samples with and without oxygen plasma cleaning.

The first cleaning step is the most difficult to characterize, as the entire gold surface is exposed and oxygen currents are overpowering. Moreover, it is difficult to study it by looking at the final sensor, since the other steps also introduce variability. Specifically, in the lab we started doubting the oxygen plasma cleaning performed on each gold die. We feared that, by using oxygen and not an inert gas, we might be introducing oxygen radicals and other impurities on the surface. Thus we prepared several samples with and without plasma cleaning and, before depositing DNA or passivating agents, we measured them in a methylene blue solution. Figure 2.1 shows the effect of the oxygen plasma cleaning in terms of impedance of the gold electrode. After fitting the circle on the highest frequencies, the charge transfer resistance is found as its diameter. The resistance value for the samples treated with oxygen plasma cleaning is on average 47 k $\Omega$  while the sample without such treatment is almost one hundred times more resistive at 4 M $\Omega$ . While this is not necessarily directly correlated with a better final sample, it suggests that oxygen plasma cleaning can effectively remove residues from gold and create a more pure starting electrode. It also suggests that using oxygen instead of a

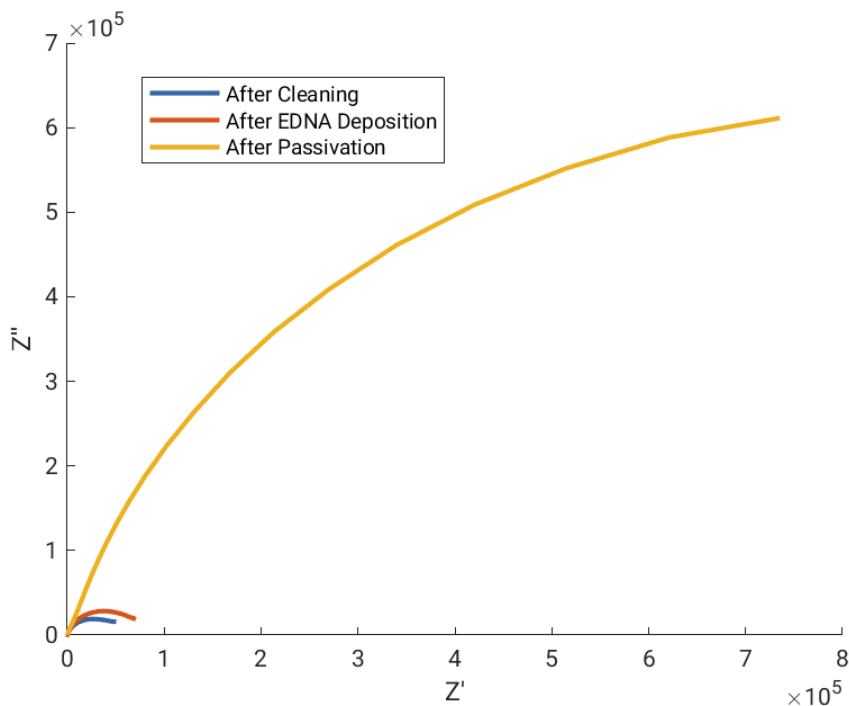


**Figure 2.2** – Impedance spectroscopy measurement of a gold electrode after each step of EDNA preparation in a 4  $\mu\text{M}$  MB in 1X PBS solution.

noble gas, such as argon or helium, does not lead to the formation of gold oxide groups on the surface, which might worsen the sample conditions and were a primary concern when establishing this fabrication protocol.

Furthermore, Figure 2.2 shows one electrode as measured after each fabrication step in the same 4  $\mu\text{M}$  MB solution. The resistance measured after cleaning is 50  $\text{k}\Omega$  which increases to 72  $\text{k}\Omega$  after EDNA deposition. As predicted, the DNA that is attached to the surface via thiols creates a sparsely populated layer that can locally interfere with electron transfer and makes the effective electroactive area of gold smaller, thus increasing the resistance, only marginally because of the low density. A drastic change is seen after passivating the electrode with mercaptohexanol, where the resistance increases to 1.65  $\text{M}\Omega$ . This is the effect of the formation of the self-assembled monolayer that covers the entire area and has the aim of making charge transfer as difficult as possible, by creating an insulating layer between the electrode and the solution.

It is worth to note that the sample not treated with oxygen plasma cleaning shows a decrease in charge transfer resistance after EDNA deposition, which could indicate that

impurities on gold are not bound to the substrate, but can be washed away during the one hour deposition time. However its resistance is still, at that point, five times higher than plasma cleaned samples and this difference is reduced with further steps. While the effect might not even be measured anymore on the final assembly, the 5x difference after DNA deposition suggests that EDNA does not see a perfectly clean surface and its density could be lower, notwithstanding the possibility that such impurities can diffuse in solution and contaminate it.

It has also been observed that, after measurements are performed in the MB solution described above, the number of methylene blue molecules increases (see Section 2.3 for the method) even after flushing and exchanging the buffer to PBS without any MB in it. This suggests intercalation of methylene blue molecules in DNA strands which is due to electrostatic interaction for ssDNA<sup>18</sup>. For this reason, performing impedance spectroscopy measurements with methylene blue in solution could be a good way of testing different fabrication conditions, but the sample obtained should not be used at the end, as they incorporate more MB than desired. Moreover MB could also intercalate at any position on the DNA strands, defeating the purpose of precisely controlling the distance from the surface. This phenomenon could also interfere with the assembly of the layers on surface and skew the data obtained, so that using ferrocyanides might be a more viable solution for DNA systems.

## 2.2 Electroactive Area Estimation

Gold surfaces prepared with different methods can appear macroscopically identical and show the same chemical properties, but the fabrication process plays a fundamental role in determining the micro and nanoscale features of the surface, yielding samples with very different roughness and profiles. When the aim is to evaluate how these different surfaces bind DNA origami, thiols or any compound, the parameter of choice is usually the density of molecules on the surface, which can be measured in different ways, for example by AFM imaging or with the techniques in Section 2.3.

However the number of molecules measured is directly proportional to the surface area and, if the aim is to evaluate the goodness of the fit of the combination gold-molecule, the differences in area due to surface roughness should be also taken into account. As a

working example, thiols may easily fill a very rough surface, thanks to their nanometric size, but DNA origami, with a radius of 100 nm, might not even feel the roughness or it could be detrimental to the binding.

It is possible to electrochemically measure the apparent electroactive surface area by exploiting a process of reduction and oxidation of the gold directly. While gold substrates are popular for their inactiveness, it is possible to force the oxidation using sulphuric acid ( $\text{H}_2\text{SO}_4$ )<sup>19</sup>. The sample (bare gold with the gasket) is placed in the cell in a solution of 0.05 M ( $\text{H}_3\text{SO}_4$ , although higher concentrations are also possible, and then scanned in voltage from -0.35 V to 1.5 V (always against an Ag/AgCl reference electrode) with a scan rate of 0.1 V/s which keeps the reaction reversible enough.

In the cathodic direction, increasing the voltage, there is a peak from around 1 V to 1.5 V which is the result of the gold molecules on the surface being oxidized, while the opposite happens in the other direction, with a very sharp peak around 0.9 V when the gold oxide is reduced back to gold. Assuming the complete reaction of all the atoms, the reduction peak can be integrated on time and that charge corresponds to the electrons exchanged in the reaction. Dividing this charge by  $422 \mu\text{C}/\text{cm}^2$ , the charge density corresponding to the oxygen adsorption, finally gives the effective surface area.

The measurement was not immediately easily reproducible as the plots were not easy to relate to the theoretical shape, with very different behaviors for different sample. One example is shown in Figure 2.3, where several unexpected peaks appear: just by looking at the reaction potential, the only peak effectively related to gold oxidation is the low one at 0.9 V, while the much more prominent one at 0.55 V is not explained without considering other contaminants. Moreover, some samples underwent sensible changes which are apparent to the eye, darkening the colour from gold to rust, which suggested that another reaction was happening at the same time, damaging the substrate. The most likely candidate was eventually identified in gold chloride that could be forming through a tiny amount of potassium chloride present in the flow cell. KCl is not a desired molecule during the measurement, but it is in the solution in which the Ag/AgCl reference electrode is stored for preservation and some of it may stuck to the glass of the electrode crystallizing and then dissolving in the cell.

Thorough cleaning of the reference electrode through rinsing and drying with a Kim Wipe was added in the process flow for all subsequent measurements, which are now

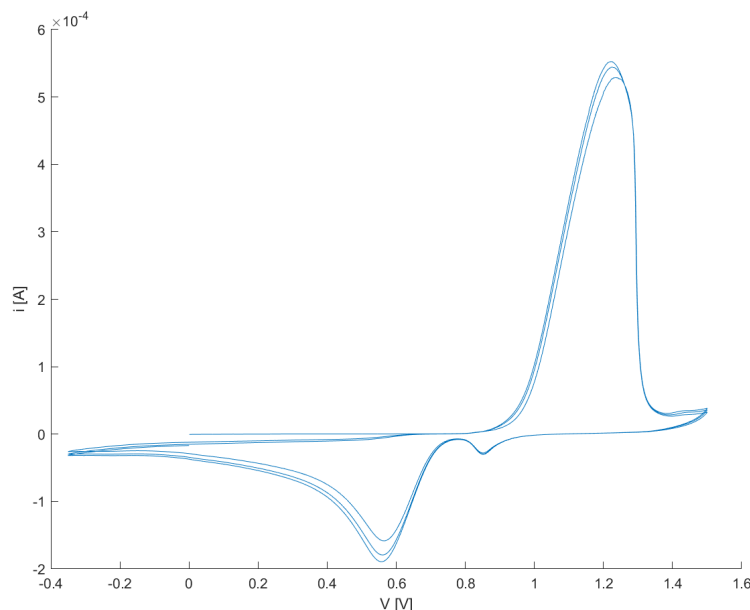


**Figure 2.3** – Early measurement of a gold sample electrochemical active surface area, showing spurious redox peaks.

comparable to the reference, although a small spurious peak is left as a shoulder to the main reduction current, as shown in Figure 2.4.

Hypothesizing that the kinetics of the two reactions might differ, a slower (0.005 V/s) measurement was run, resulting in Figure 2.5. As the parasitic reaction becomes more reversible, its potential is also shifted further from the other peak of interest. Separating the two peaks was successful using this method and the integration was more reliable. Furthermore, reparing the sulphuric acid solution temporarily solved the problem. While these other peaks are most certainly related to some degree of contamination of the solution, it has not been possible to find a way to consistently prevent them and another method has been used.

Specifically, after the measurement is performed, the integration of the charge is performed with a MATLAB script that first fits the gold oxide reduction peak to a unimodal distribution and then performs calculations on it, removing the contribution due to any other reaction.

A previous section should describe the different gold types

Three different types of gold substrate have been tested, electron beam deposited gold on a titanium substrate, lab-made template stripped gold and commercial template stripped

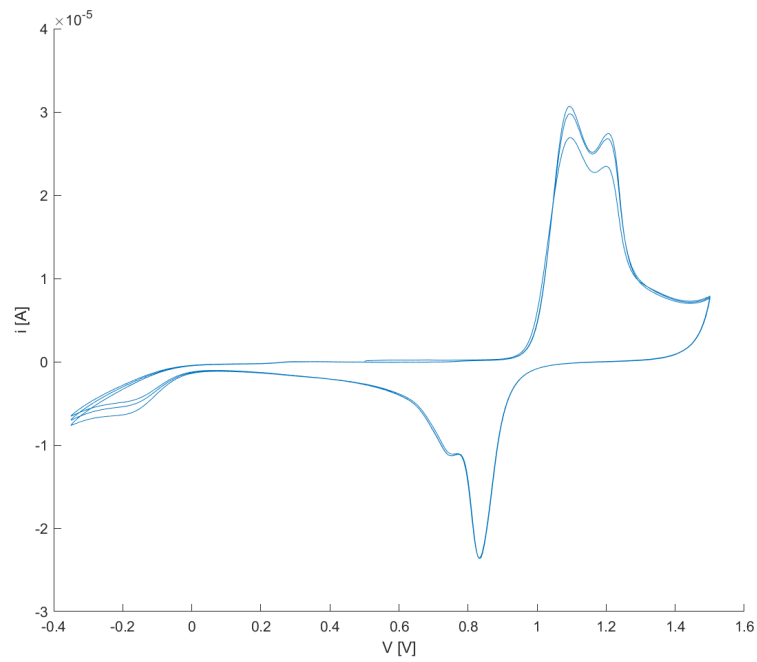


**Figure 2.4** – Cyclic voltammetry measurement of a gold electrode in 0.05 M  $\text{H}_2\text{SO}_4$  after cleaning the reference electrode.

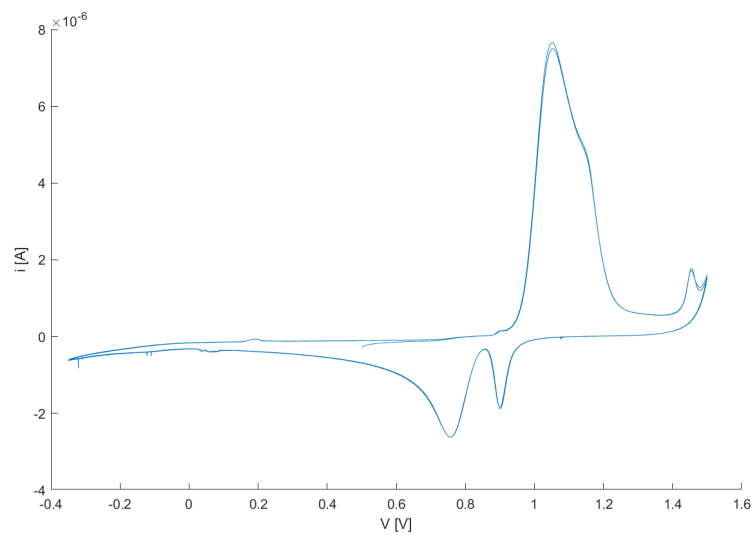


**Figure 2.5** – Cyclic voltammetry measurement of gold surface performed at a scan rate of 0.005 V/s.

gold (Platypus), with the results shown in Table 2.1. The nominal area is calculated starting from the silicone gasket size (2 mm in diameter) and the table reports the difference factor with respect to this nominal area for measurements at both 0.1 V/s and 0.005 V/s.

**Table 2.1** – Difference between effective electrochemical surface area measured and nominal area for different gold samples at two scan rates. The integration is performed both on the raw data and on the Gaussian fit to remove spurious peaks.

|       | 0.1 V/s | 0.1 V/s fitted | 0.005 V/s | 0.005 V/s fitted |
|-------|---------|----------------|-----------|------------------|
| TiAu  | 2.86x   | 2.5x           | 2.9x      | 2.9x             |
| TsAu  | 2.1x    | 1.8x           | 2x        | 2.3x             |
| Platy | 2x      | 1.8x           | 1.7x      | 1.7x             |

When probes with a small area are used, as in the EDNA experiment, it is useful to increase the surface area several times beyond the nominal value as the thiols will effectively see a larger surface and be more densely packed, resulting in more probes on the same amount of gold, allowing higher miniaturization, lower costs and improved signal. However, if the probes have a larger surface, such as the DNA origami employed here, the gold electrode should be as flat as possible to allow to stick in the correct position, thus forming the strongest interaction with the substrate and avoiding possible

### 2.3 Probe Density

Being able to fill a surface with more probes means being able to have a smaller sensor with the same results in terms of output. Miniaturization then allows to cut costs in a quadratic way and is one of the very reason for the development of several nanotechnologies. For example e-beam lithography allows to increase the resolution to 10-20 nm<sup>20</sup> from the 50 nm given by photolithography while the cost of a mask increases to millions of dollars. However the shift to the new technology has proven convenient, thanks to the consequent increase in density of transistors, which makes up for all additional costs. To improve and evaluate this parameter, it is fundamental to be able to obtain an estimation of the density of probes on the surface. One easy technique to do so is to count the number of structures in a certain area with an AFM measurement, provided that they

can be clearly resolved and are firmly bound to the substrate. There are however drawbacks to this: the sampled area might not be representative and human count is tedious. Furthermore, as mentioned above, some molecules as the EDNA strands are very hard to see under AFM and the final method is unreliable, when not entirely inapplicable. Electrochemical procedures, on the other hand, are able to detect a molecule as long as it participates in the reaction and contributes to the current, however there are other factors that come into play and should be removed. The contribution due to non-faradaic effects and oxygen currents is always present in each of the techniques described in Section 1.2 and must not be mistaken for signal.

One of the most straightforward ways to do so is to extract the information from the AC voltammogram<sup>21</sup>, where the total number of molecules involved ( $N_{total}$ ) is given from the measured peak current ( $I_{avg}$ ) according to the relation:

$$I_{avg}(E_0) = 2nfFN_{total} \frac{\sinh(nFE_{ac}/RT)}{\cosh(nFE_{ac}/RT) + 1}$$

where  $E_0$  is the standard reaction potential,  $n$  the number of electrons involved per each molecule (2 for methylene blue),  $f$  is the frequency of the signal,  $F$  the Faraday constant,  $E_{ac}$  the amplitude of the AC signal,  $R$  the universal gas constant and  $T$  the temperature. While this method has been used frequently for these systems<sup>22</sup>, the same group has later noted that the result is also dependent on the geometry of the system<sup>23</sup> and the results seem to be correlated, but not equal in absolute value, to other, more reliable methods. The preferred<sup>23</sup> way for EDNA probe density estimation is through chronocoulometry<sup>24,25</sup>, a technique that measures the dynamic current response of a single applied voltage step. The current has a decreasing exponential behaviour where the asymptotic value contains information both on the background noise and on the number of molecules. To be able to discern the two, it is however necessary to perform two different measurements, one without redox indicators and one with a redox active solution. The first measurement, without redox indicators, is performed simply by using a plain buffer and running a sample chronocoulometry. The second measurement, instead, requires free redox indicators in solution. This leads to a completely different setup, where hexaammineruthenium(III) chloride (RuHex) molecules dispersed in solution stoichiometrically bind to DNA helices and give rise to an electrochemical signal that indicates the volume of bound DNA. This

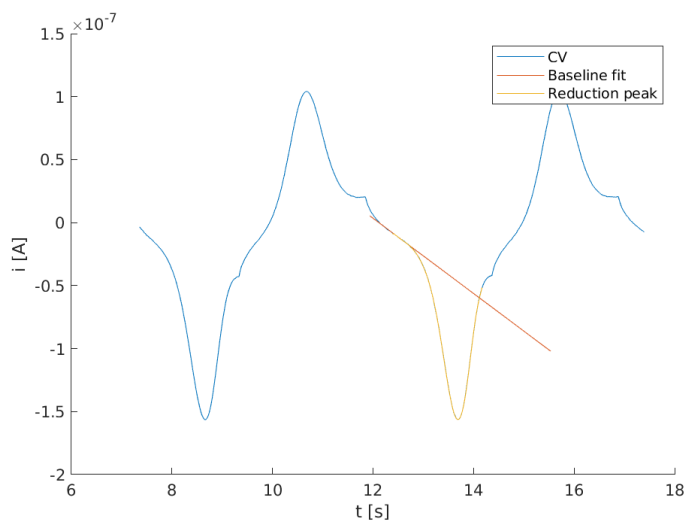


**Figure 2.6** – Example of a cyclic voltammogram of methylene blue labeled EDNA (in 1x PBS) plotted against time.

would not be a suitable process for DNA origami structures because it has never been proved that the same stoichiometry is valid for these complex and folded nanostructures, thus there is no way to correlate the data.

In cyclic voltammetry it is assumed that all the methylene blue molecules are reduced and oxidized, transferring two electrons each. The number of electrons can be reconstructed by plotting current over time, and integrating as:

$$\int i dt = \int \frac{dq}{dt} dt = Q$$

To remove the unwanted contributions, a baseline can be selected by approximating the background to a line. The most common way to do this in literature is to select a relatively flat section of the anodic curve before the peak and then extend it until the other tail. Figures 2.6 and 2.7 show the application of this method on a sample with methylene blue labeled EDNA in a 1x PBS solution. The main limitation of this technique is readily evident and lies in the uncertainty of the baseline: it looks as though the point where the fitted line and the peak tail intersect is still far from the real end of the tail. However using a larger part of the curve would mean, after subtracting the baseline, having values for the current of opposite sign which would end up reducing the result of the integration. Of course there is no physical interpretation of removing this charge as the molecules should all simply add up.

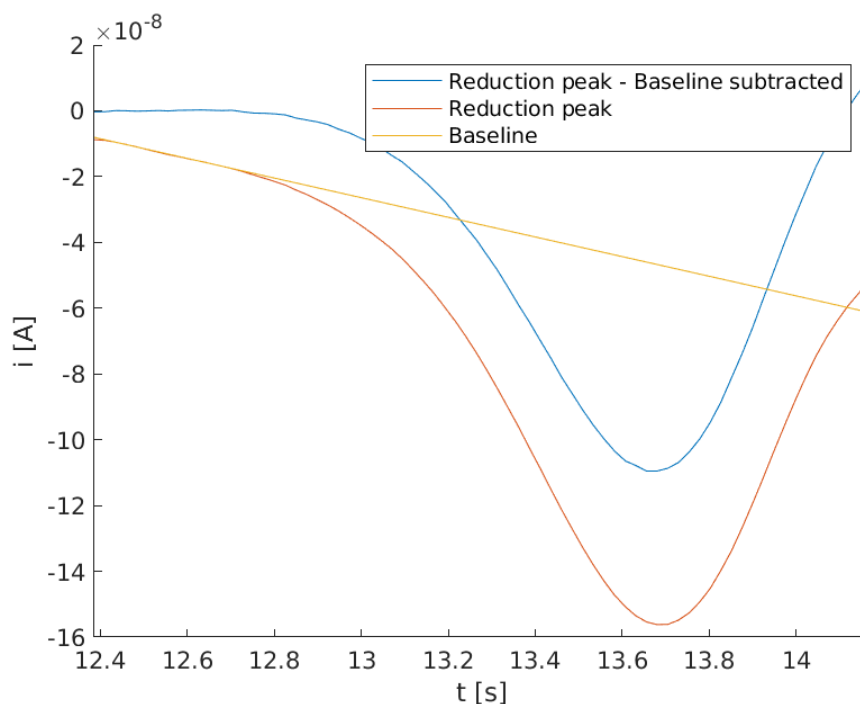


**Figure 2.7** – Peak and baseline of Figure 2.6 with the final baseline subtracted peak.

The only way to properly subtract the non-faradaic effects would be to measure the system in the same voltage range without the redox indicators. In these setups it is not possible to remove methylene blue and isolate its effect, as the EDNA is already functionalized with methylene blue and is deposited before the passivating agent. Another possibility, if the passivation layer was sufficiently reproducible between different samples, would be to have one sample without probes and obtain the background signal from that. The idea has been tested, but the residual background currents after passivation have a variability between different samples that would lead to errors much higher than those due to an imprecise baseline selection.

## 2.4 Electron Transfer Rate

To obtain information about the geometry of the system, dynamic measurements are performed, in order to extract the electron transfer rate, that corresponds to the number of electrons exchanged per unit of time. The probability of tunneling for an electron follows a formula that can be written as:

$$T(x) = Ae^{-\alpha x}$$

where both  $A$  and  $\alpha$  take into account the properties of the potential barrier and the energy of the electron.  $x$  is the size of the barrier, in this case the distance between the MB molecule and the gold electrode. Thus the probability of tunneling decreases exponentially with increasing distance and the rate of electron transfer ( $k$ ) will be affected in the same way.

While more information is required to exactly quantify the distance, qualitative knowledge of the kinetics can be extracted from this value, all the more so knowing the expected geometry of the probes.

Only measurements that move the system out of equilibrium can peek into its dynamic properties, as it must be studied in its most extreme condition, when it is limited by the transfer rate and not by other phenomena such as diffusion or the possibility of easily reaching another equilibrium. This means that significant voltage steps have to be applied, instead of progressively sweeping different voltages as in cyclic voltammetry. Otherwise, if CV is chosen for this, the scanning rate must be fast enough that the peaks start splitting (showing irreversibility) and the redox reaction still cannot keep up with the potential change applied by the potentiostat. From here, an “apparent” transfer rate can be extracted<sup>26</sup> and it can be correlated to the actual transfer rate if assumptions on the reversibility of the reaction are made<sup>a</sup>.

One of the most successful techniques is to simply apply a high enough potential step and measure the current response of the system. The resulting measurement has very strong background currents due to the non-faradaic processes happening when the voltage is changed, but, after averaging hundreds of such plots, post-processing can extract a precise value for the transfer rate, with a resolution of hertz<sup>27,28</sup>. However this requires a long time to perform all the measurements and we do not have a clear understanding of the final processing of the information.

The technique we decided to use exploits the ability of square wave voltammetry to screen the background signal by subtracting the forward and reverse currents. One of the parameters in such a measurement is the frequency at which it is performed (one over

---

<sup>a</sup>Two parameters are missing:  $\alpha$  and  $\gamma$ . While  $\alpha$  is an important parameter that signifies how symmetric the energy barrier is (cf. [9] Sec. 3.3.4), in most cases their combined effect is negligible and the apparent transfer rate equals the actual one.<sup>26</sup>

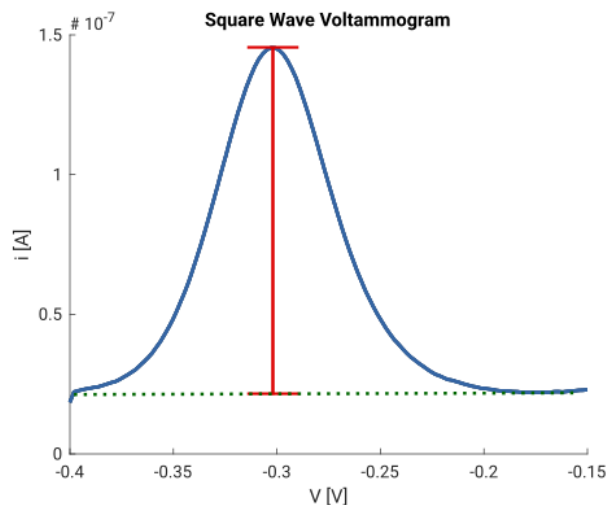


**Figure 2.8** – Square wave voltammogram with the extraction of the peak current highlighted. The baseline is automatically found by the measurement and analysis software (NOVA).

the step size) and there is a correlation between the peak current obtained at a certain frequency and the electron transfer rate<sup>29,30</sup>. The peak current can be extracted as in Figure 2.8 and, after sweeping on a wide range of frequencies (few hertz to a kilohertz), a Lovrić plot is created with the logarithm of the frequency on the  $x$  axis and peak current divided by frequency on the  $y$  axis, as in Figure 2.9. Such a plot visually presents a peak in current and the position of its maximum is the apparent transfer rate. To obtain the actual transfer rate, this value should be divided by  $1.02 \pm 0.14$  (for a step size of 50 mV and common values of  $\alpha$ , cf. Footnote a).

A technical note is necessary before proceeding further. It is been mentioned in Paragraph 1.2.5 that, in square wave voltammetry, the currents, forward and reverse, are measured at the moment just before inverting the step. of course this is ideal and different instruments will have different tolerance as point measurements are not possible. Many potentiostat makers have gone beyond this and started to implement different sampling methods, ranging from a single point to the average of the entire step<sup>31</sup> in order to improve peak currents and signal to noise ratio. This, we verified, has led to inconsistent and unreliable values when Lovrić plots are used for electron transfer rate extraction. These findings are reported in Appendix ?? for their importance and common interest, but they are outside the main scope of this work. However it is important to note that the values given here for electron transfer rates can only be compared between each other,

Add appendix

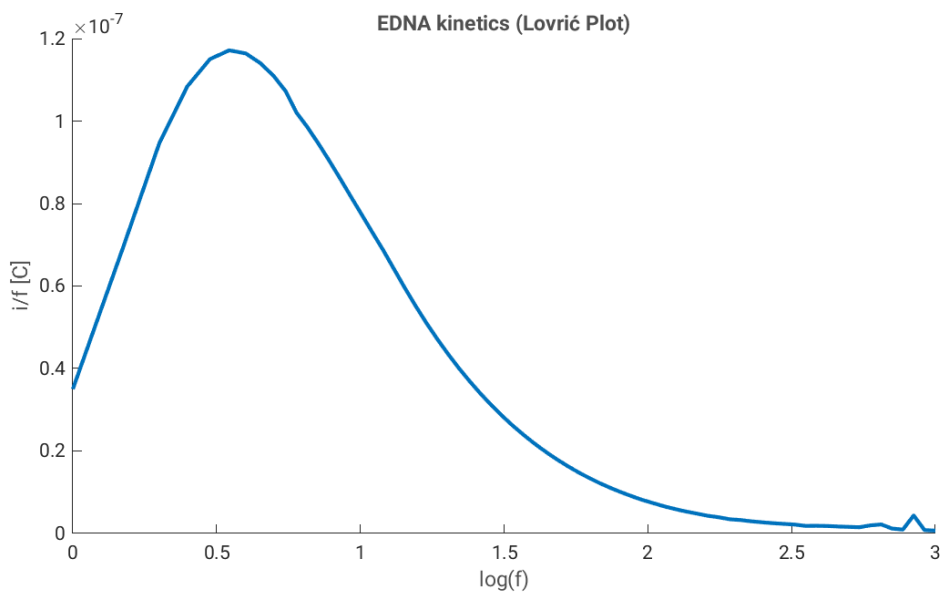


**Figure 2.9** – Lovrić plot formed by extracting the peak current (divided by frequency) for a large number of frequencies. The final dimension of a charge is purely theoretical and does not imply physical meaning

not against other published works using different instruments.

## 2.5 Surface Passivation

While gold is considered an inert substrate with little to no participation in chemical or electrochemical reactions, this is not always the case, as shown in Section 2.2, for instance. Another phenomenon is the oxygen current developed on gold at sufficient low voltages (around 0.45 V vs Ag/AgCl reference electrode), this current grows with decreasing voltages and its absolute value increases rapidly enough to shield any other signal with what is considered just background noise.

This oxygen current can be inhibited by covering the gold electrode with a passivating layer that decreases the surface area exposed to the electrolyte solution. This is obtained with self-assembled monolayers (SAM), thiols that form closely packed assemblies on gold. Thiols are organic molecules with an alcohol tail and an SH group head that can be chemisorbed on gold creating a strong binding. When other structures, such as DNA origami, are deposited on the electrode, a SAM can be used to backfill it and completely cover the free area in between the UNKNOWN.

maybe move this somewhere earlier

Thiols are classified based on the length of the alcohol tail, for example 2-mercaptoethanol, where mercapto indicates the sulfuric group and ethanol is the primary alcohol. By changing this tail, several molecules are possible with longer alcohols and chain as long as sixteen CH<sub>2</sub> group (1-hexadecanol) are available commercially<sup>32</sup>.

The length of the alcohol tail influences the kinetics of the system in EDNA sensors: the taller the passivation monolayer, the further the DNA strands are kept from the surface and the lower is the tunneling current of methylene blue. For this reason two different alcohol chains have been tested, a six chain, 6-mercapto-1-hexanol and a shorter three chain, 3-mercapto-1-propanol.

Thiolated alcohols are neutral molecules, with no charge, thus a SAM cannot be compared to the usual substrates onto which DNA origami is bound, where the common property is a negative surface charge that allows for divalent cation binding between the DNA and substrate. It is however possible to recreate this property by using carboxylic acids, which are characterized by an OH negative group on the end of the tail. Each alcohol has a corresponding carboxylic acid and its thiol. Two different molecules were tested, with the same lengths as those used for alcohol chains: 6-mercapto-1-hexanoic acid and 3-mercapto-1-propionic acid. While the monolayers formed by these thiolated

acids could favour the binding of DNA nanostructures, their charge is expected to interact with the process of electron tunnelling of the redox indicators and affect the kinetics of the system.

Complete section:  
CVs and SWVs that  
confirm this

# Labelling of DNA Origami with Methylene Blue

## 3.1 Auxiliary Structure Design

The DNA origami sensor proposed in Paragraph 1.3.3 is the long-term goal of this project, for it may be able to overcome some of the limitations of current systems, as explained. However it also presents several critical steps that have not been reached at this point. One example of such difficulties is the fact that the structure requires a two part origami, one bound to the surface, one free to move in solution and attached only via a long flexible linker. If this was to be designed as a single scaffold origami, it would require a very long starting scaffold strand, more than double with respect to what is commonly used, as each of the two parts could be a stand-alone origami. Longer scaffolds are not easily commercially available, although there are studies in this direction<sup>33,34</sup>, as they are difficult to clone and the synthesis yield is lower. The envisioned way is to attach together two separate pre-assembled structures via sticky ends hybridization, but this adds one extra layer of complexity. A maybe bigger challenge is that, of the two parts, only one should have some affinity for the surface and stick onto it, while the other one should feel no binding force and be able to float in solution. It is possible to have a more or less sticky substrate, but, in this case, the structures themselves should be functionalized to selectively bind on the same surface.

To be able to start working on the heavy loading of DNA origami with methylene blue while these other challenges were investigated at the same time, a simpler structure was devised, one that could still ideally perform sensing operations, but only by sacrificing

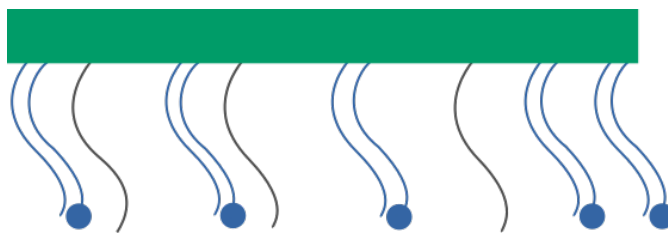


**Figure 3.1** – Methylene blue labelled origami design

some of the advantages of the other design. Figure 3.1 shows the origami itself, viewed from the side, while Figure ?? shows the cadnano design from the top. Under the main structure there are several tails, that are staples extended with a fixed sequence, that will bind to a methylene blue labelled strand, in order to have the redox indicator directly below the origami. Then a few other staples (called surface binding) are extended with a different sequence that, during the annealing process, is left single stranded without its complement. Figure 3.2 shows the role of these tails: they can hybridize to another strand that has been attached to the gold substrate with a thiol. These tails however are not entirely complementary to the surface bound oligonucleotides, there is a 5 nt long toehold, so that an invader with perfect complementarity could displace them and free the origami from surface, releasing it back in solution, as per Figure 3.3. Such invader is the analyte strand: before it is added to the system, the origami are on the surface and MB is within electron tunnelling distance, so a faradaic current can be read. When the target analyte is added, the origami are released, the surface binding sites are occupied and, after flushing, no MB should be present anymore in the system, giving ideally a zero current.

We still expect to see a signal from structures that might be less accessible to the invader strand, but the most significant part should be correctly displaced and can be flushed away by rinsing the cell. The surface is now almost completely regenerated and incubation with new origami can recreate the sensor for a second measurement. This situation is not ideal as the origami, the most advanced and expensive part of the setup, have to be flushed away and new ones are used each time, so this is part of the trade-off in this system. A solution to this will be discussed further on.

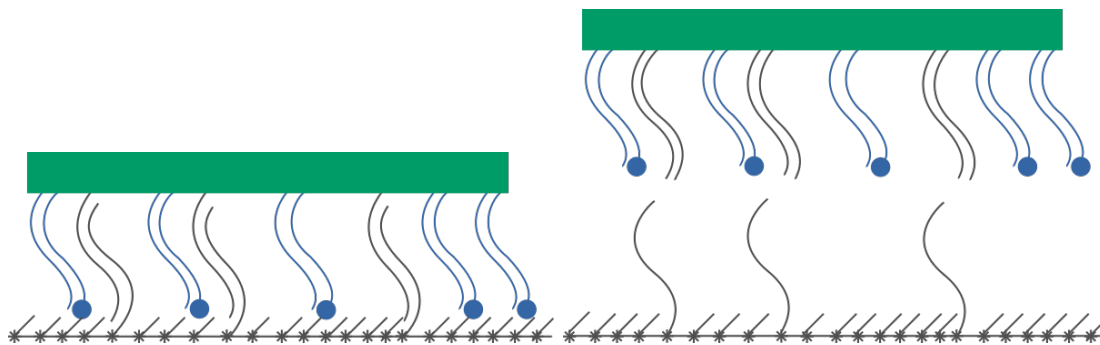


**Figure 3.2** – DNA origami bound to surface. **Figure 3.3** – Invaded origami released from surface.

### 3.2 Death star design with 30 surface binding sites and 98 methylene blue sites

The first design was exactly the one described above, after choosing how many staples should be extended with labelling sequences for both methylene blue strands and surface bound oligos. For the thiol binding, 30 staples were modified in order to have a structure that adheres strongly to the surface so that it would not wiggle, or worse be detached, by small perturbations, such as the AFM tip. However, having 30 sites where the origami is attached to the electrode also means that there need to be 30 displacing oligos to release one single origami and see a change in signal, affecting the detection limit of the sensor. The number of staples extended for methylene blue is an important parameter as it is correlated to the amplification of a binding event, if there are 30 MB molecules on a single origami and 30 analyte molecules are needed to release it, the final change in signal will be one MB molecule per each analyte molecule, as it is the case for usual EDNA sensors. On the other hand, if one were to label each origami with, for example, 180 MB molecules, the gain would be six times higher. There are 234 total staples in this design, which means that, after using 30 for the surface binding, one could theoretically have 204 methylene blue molecules. Such a heavy loading has not been well studied and is one of the final goals, but possibly not a good starting point. Instead this design was chosen according to the surface density of EDNA in previous experiments, in order to obtain measurable currents. EDNA has been measured in concentrations around  $1E11$  molecules/cm<sup>2</sup> (upper limit around  $1E12$ /cm<sup>2</sup>), which translates to approximately 1 MB

molecule per  $10 \text{ nm}^2$ . These DNA origami are round with a diameter of 100 nm, which means that, assuming full packing, labeling them with 100 molecules of methylene blue could achieve similar currents, hence the 98 extended staples (two were dropped for other limitations).

The origami can be approximated as a planar structure and it has been designed and optimized (with the website CanDo<sup>35</sup>) to minimize the stress and remain flat. This means that designing longer staples for surface binding or MB labelling needs to take into account the side from which they will be extended, but, thanks to design choices, all staples (except maybe those at the very edge) have the 5' end on one side and the 3' end on the other side of the origami.

Furthermore modifications of DNA strands, such as ammine groups for MB labelling or thiols can be performed on either end, but have a much higher yield if done on the 3' end as this is the starting point for DNA synthesis. The process is not perfect, which means that many strands will be truncated before all the correct bases have been added and 5' end modifications can be done only on strands that are perfectly synthesized. Additionally, if a strand is truncated at 19 bp out of 20, it will not have a 5' modification, but it will still bind to its complementary on the origami and detrimentally occupy one site. However, if the modification is on the 3' end, it will still be truncated and occupy such site, but it will also have been correctly modified and will add one MB molecule to the origami as desired.

This shows how it is advantageous to have both the thiolated strands and the MB strands modified on the 3' end and this also means that the staples should be modified on the 5' end so that the two can hybridize correctly as in Figure ?? . For this reason the 5' side of the origami will consistently be the one on the bottom closer to the surface and the 3' side will be on the top, further away. In the next sections other kinds of placement will be discussed, when they may be theoretically advantageous, but it is straightforward that having both on the same side can bring the redox molecules as close as possible to the surface, which is one of the end goals.

find figure or re-  
move ref

### 3.2.1 Annealing and purification of the origami

This paragraph describes the annealing and purification process for the origami with 98 MB sites and 30 surface binding sites, but the process is general and will be applied for any subsequent origami design, without describing the procedure again.

The first step is the preparation of the staples mix, the tube with the whole set of staples in the same concentration. The staple oligonucleotides are synthesized all separately and delivered in plates, each well then contains a different staple diluted to the same concentration. All the required staples are pipetted in a test tube from the different plates. There are different sets of staples mixed together: the unmodified sites (106 staples), 98 staples extended by 20 nt with the sequence complementary to the MB strand, 30 extended by 25 nt with the 20 nt sequence complementary to the thiolated strand and a 5 nt toehold for displacement.

The origami mix is then prepared with scaffold, staple mix and buffers. The scaffold is used here at a concentration of 20 nM while the staple mix is used at a concentration of 50 nM per each strand (2.5x with respect to scaffold). The concentration of surface binding oligos is x the one of the staples, to have 1x excess to the total number of sites. Every origami anneal is done in a buffer of 1x TAE and 12.5 mM MgCl<sub>2</sub> which keeps the DNA stable with pH control and positive Mg ions.

Wrong

Before incubating with the MB strands, the last step is the purification of the sample by use of a commercial ultracentrifugal filter, with a cut-off size of 50 kDa. The sample in the filter is centrifuged and the membrane lets everything under 50 kDa (the staples) flow through and retains the DNA origami.

To estimate the yield of recovery, a spectrophotometer is used to measure its concentration. DNA absorbs light at a wavelength of 260 nm and the absorption is proportional to its concentration in solution. However the absorption is different for single and double stranded DNA and depending on the base, so it is possible to exactly calculate the absorption of each single DNA origami unit, its extinction coefficient. Measuring the absorbance of a sample and dividing it by this value<sup>a</sup> gives the final concentration of origami in the tube. The sample was then incubated for one hour with the MB labeled

---

<sup>a</sup>The measuring pathlength must also be taken into account but it is set at 1 cm to provide normalized data

strands for one hour. After running an agarose gel after 1 h incubation, the sample had seemingly disappeared and the origami band could be seen only with very high contrast, which also revealed the presence of dye stuck in the loading wells. This is mostly likely due to the origami aggregating and forming structures so large that the applied voltage did not prove strong enough to force the sample through the wells walls and into the agarose gel pores.

The next logical step was to directly anneal with the methylene blue strands, so that the tails would never be single stranded on the origami and might have less interaction with each other. The agarose gel, shown in Figure 3.4, suggests once more that the origami are aggregating as the signal from the dye can be seen only in the wells. It is clear how the band for the correctly formed origami is remarkably dimmer for the samples with MB, however another possible explanation of this is the quenching of the dye used for electrophoresis (SYBR Safe) due to interaction with methylene blue molecules. This would mean that the origami are there, but they do not show up under the scanner because the dye is silenced. Further experiments will also try to disprove this claim, at least disprove that MB completely quenches other dyes.

Two explanations of this phenomenon are possible, considering that the origami without tails folds correctly: the aggregation could be caused either by methylene blue molecules or by the very tails on the origami. To test this idea, the same structure was used but the tails were changed. Instead of annealing the origami with the MB labeled tails, another oligonucleotide was used with the same sequence but without the MB molecule at the end. Four different samples are folded and run in the agarose gel (Figure 3.5): the first one is the origami with single stranded tails and no complementary strands, while the other three have the complementary strand in different values of excess to the concentration of tails. In this case the gel shows well formed origami for all the lanes and there is also a clear difference in running distance (how far from the wells the band is found) between the origami with single stranded tails and the others, meaning that the double stranded tails make the whole structure larger and heavier, as expected since these increase the total size.



**Figure 3.4** – Agarose gel (imaged at 532 nm) of different samples before and after incubation of the origami with strands labeled with MB complementary to the 98 tails on the origami itself. A 1 kbplus ladder is run in the first lane for size reference.

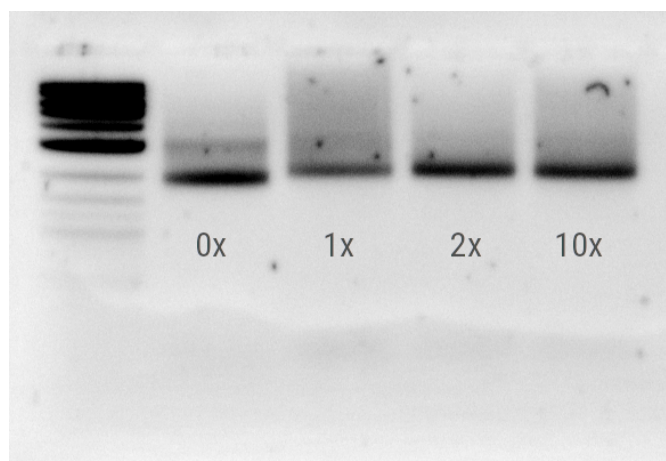


**Figure 3.5** – Gel (imaged at 532 nm) of the 98-30 sites design using tails without any MB in various excess. First lane is a 1 kbplus DNA ladder.

### 3.3 Effects of Methylene Blue Density and Concentration

As explained, the first annealing of the origami was done with 98 sites for MB strands and 30 sites for surface binding, with a scaffold concentration in solution of 20 nM, but every iteration always showed significant aggregation with structures that did not manage to leave the wells in the agarose gel.

The next step was to anneal at lower concentrations, which means both less origami per volume and less MB molecules per volume. MB has a positive charge on each molecule that might electrostatically bind to the negatively charged DNA, for example MB from one origami may bind to the DNA on another origami, thus aggregating them. Reducing the concentration could make this more rare and yield better formed structures. The gel in Figure 3.6 shows different annealing concentrations, from 1 to 10 nM (20 nM has been shown to aggregate) and proves that aggregation increases with concentration and that origami annealed at 1-2 nM are well formed enough that they might be used. 2 nM was chosen as test concentration to avoid having too low concentrations after purification (even just 1 nM is shown to reproducibly cover the entire surface on mica). Purification was performed via density gradient ultracentrifugation. The peculiarity of this technique lies in the test tube that is filled with a linear sucrose gradient from 10% to 50%, which creates a density gradient inside the tube. The DNA origami and staples mixture is then added on top of it, where sucrose is at 10%, thus lower solution density, and the sample is spun in an ultracentrifuge for two hours. The DNA diffuses, according to its hydrodynamic radius and density, along the gradient until it reaches its equilibrium position. Then the solution is pumped out from top to bottom and distributed in different

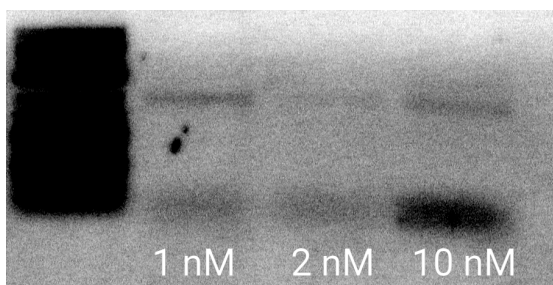


**Figure 3.6** – Gel (imaged at 532 nm) for the annealing of the 98 MB sites origami at different concentrations of scaffold, 1, 2 and 10 nM

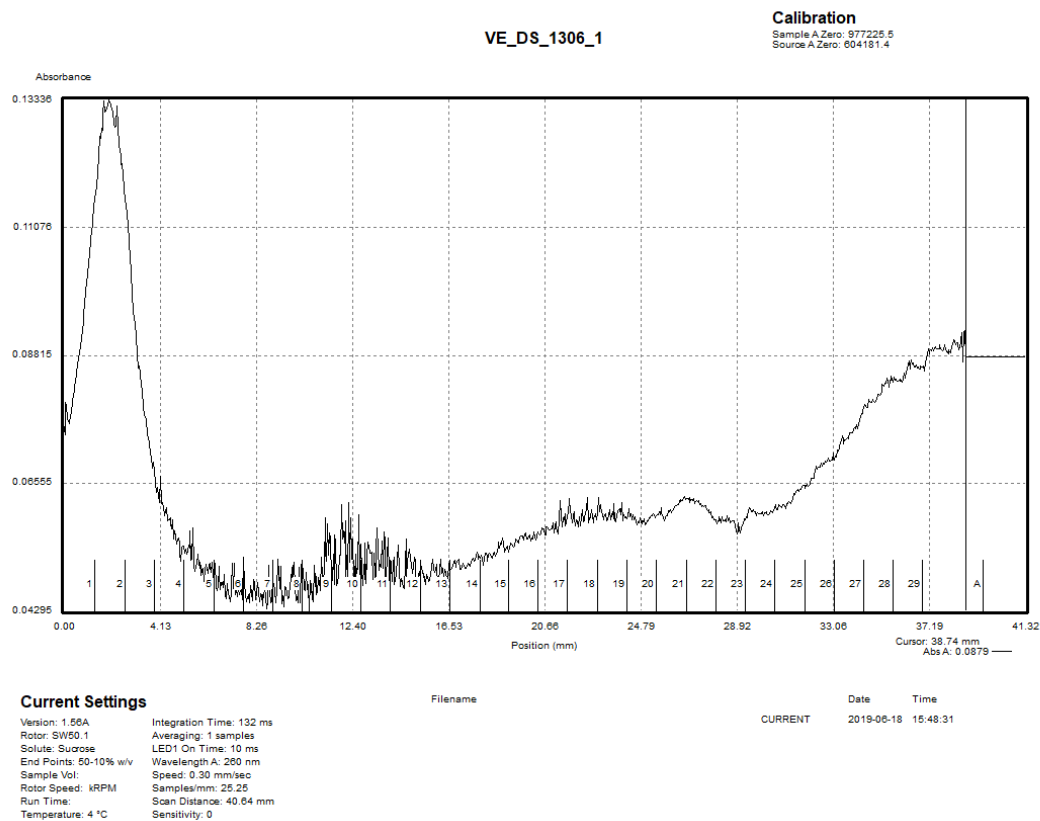


**Figure 3.7** – Absorbance measurement at 255 nm on a 98 MB sites origami after sucrose gradient ultracentrifugation. The x-axis corresponds to the position along the gradient that is being measured and the gradient starts on the left with structures with lower density (the peak due to staples) and moves in the direction of higher density. Between 21 mm and 29 mm, where origami are usually found, there is no significant peak.

test tubes, while measuring the absorbance to estimate DNA concentration along the gradient. Staples are expected to be found at the very beginning thanks to their small and flexible size, while origami should be found much later and aggregates might not even be seen (the heaviest fractions are not collected). Figure 3.7 shows the absorbance (at 255 nm) for this experiment. This seems to show almost no origami peak (compared to very high staples peak at the beginning) and it is not immediately clear whether they are present or go unnoticed<sup>b</sup>. To test this, a gel (not shown) is run using the fractions

<sup>b</sup>Previous measurements with absorbance spectroscopy seem to indicate that there is no interaction between the absorbance spectra of DNA and methylene blue. Thus it is reasonable to believe that origami would show on the profile, although the absorbance could also be affected by the very high local density of MB on a origami, while measurements have been performed on DNA strands with few

footnote with bad formatting, possibly too long for now or forever?

most likely to contain DNA and indeed this is confirmed, although the brightness of the bands is extremely low, pointing to picomolar concentrations.

Nevertheless, we decided to prepare samples for AFM, to verify the formation of the origami and whether they could be used for electrochemical experiments. Two substrates were used, one is mica, where origami stick through the double positive charge of magnesium ions, the other one is template stripped gold. This has been functionalized with the thiolated strands that bind the origami (300 nM) and then passivated with mercaptohexanol. Without the passivation layer, origami would stick on gold as they do on mica, with it they only stick through hybridization with the thiolated strands. Figure 3.9 shows the phase image for mica, while Figure 3.8 shows the phase image for gold. Both of them exhibit a very low origami concentration, less than 10 in a 25  $\mu\text{m}$  area for gold and a comparable number for mica. This again suggests that annealing with a scaffold at 2 nM, after purification, yields samples that cannot be really used, so that being able to overcome the aggregation problem is of the utmost importance.

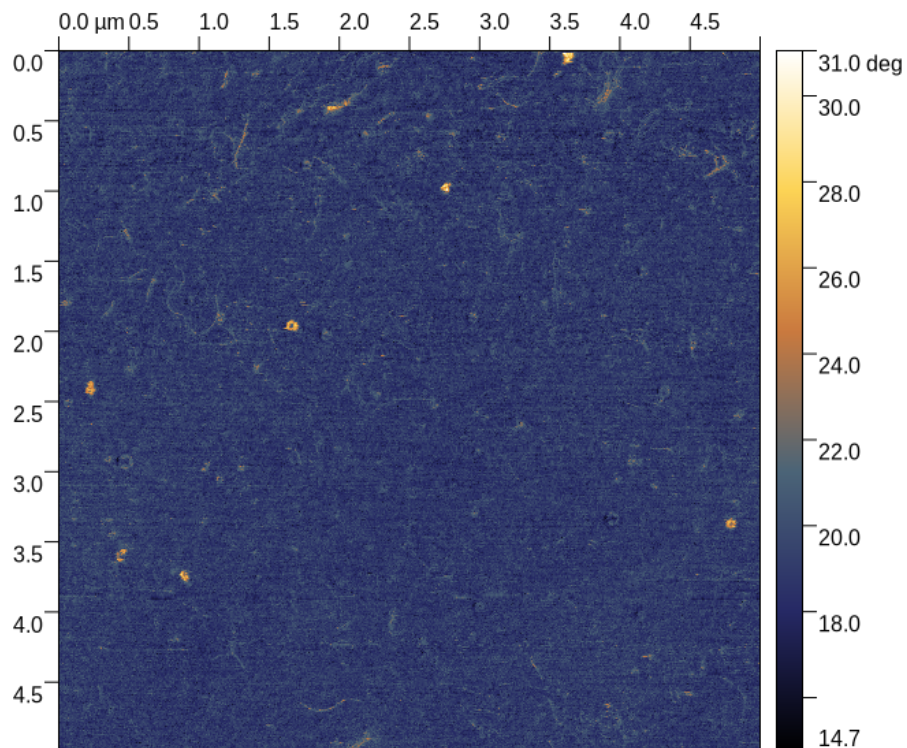


**Figure 3.8** – AFM phase image of a 98 MB sites origami annealed at 2 nM, after density gradient purification, on a template stripped gold sample functionalized with thiolated strands and passivated with mercaptohexanol.

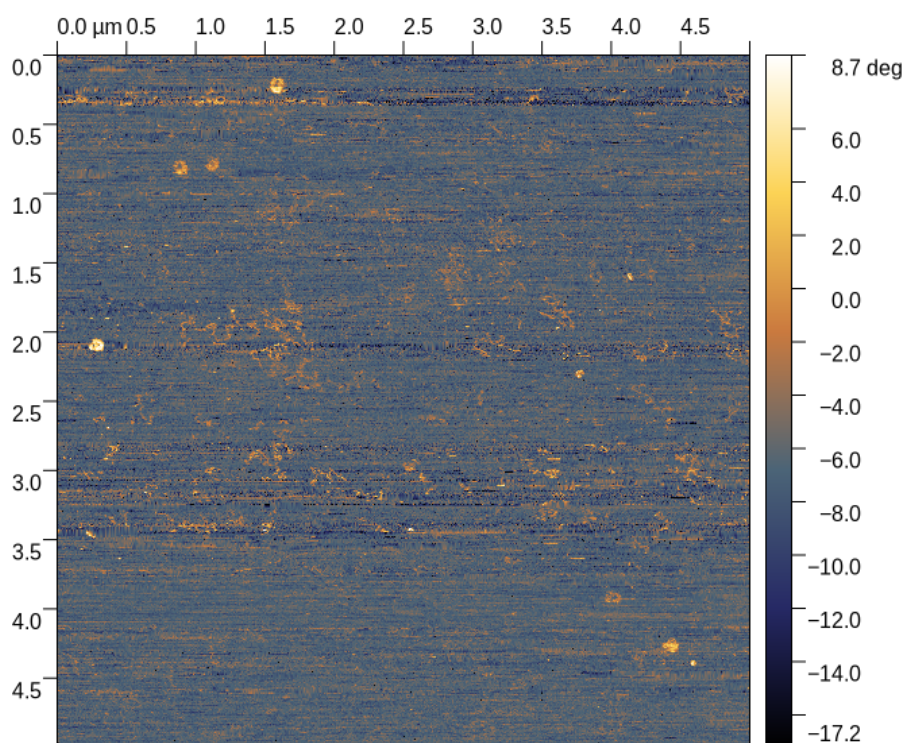


**Figure 3.9** – AFM phase image of a 98 MB sites origami annealed at 2 nM, after density gradient purification, on a mica sample

### 3.4 Reduction of Methylene Blue

It has been mentioned before that one of the causes of aggregation for MB labelled DNA origami might be the uncompensated positive charge on the methylene blue molecules, but methylene blue can exist in two forms. The redox reaction used for sensing is responsible for this and reducing methylene blue transforms it into leucomethylene blue which is a neutral molecule where the charge has been compensated. Thus reducing the MB strands before annealing might alleviate the aggregation and increase the yield of well formed structures.

Several agents can be used to reduce MB successfully, for example ascorbic acid or TCEP (Tris(2-carboxyethyl)phosphine hydrochloride) and this is clear in solution even by eye, as the leuco version is transparent compared to the bright blue of the oxidized molecule. The most commonly used buffer for origami is TAE/Mg, where TAE is a solution of Tris, acetic acid and EDTA. Unfortunately, buffering the reduced strands with TAE oxidizes them back to methylene blue and the solution turns bright blue again. Of several buffers

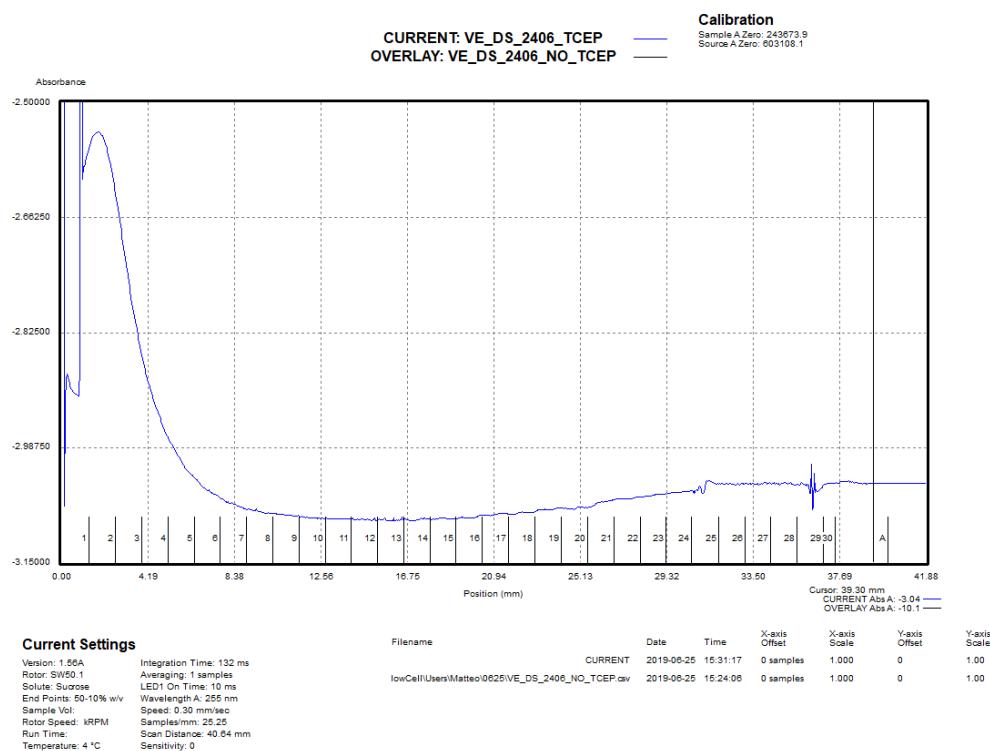


**Figure 3.10** – Absorbance measurement at 255 nm on a MB-labelled origami after sucrose gradient ultracentrifugation. An origami peak would be expected between 21 and 29 mm, while the following points are aggregates or other structures of no interest.

available in the lab, the only buffer that was found not to initiate this reaction was Tris. Adding magnesium chloride is fundamental for the origami folding and stability and does not seem to promote reoxidation, so that a Tris/Mg buffer can be successfully used.

We have not however been able to run agarose gel electrophoresis in plain Tris buffer and thus the confirmation of structure formation must be done differently. Here sucrose gradient ultracentrifugation was used to purify the origami and, during purification, the correct formation can be checked. Again, the final product of this purification method will be a tube in which the DNA material has been separated depending on its density and the relative concentration of each fraction can be measured by absorbance readings. In Figure 3.10 is plotted the profile read for the sample of origami with reduced MB, showing that there is no discernible peak for origami, while the staples are regularly measured.

This data suggests that the role of MB in the aggregation of DNA origami is not due to

electrostatic interaction, but to weaker interactions. Specifically we believe that it stems from the  $\pi$ -stacking between the aromatic rings in DNA and MB. This is also supported by the knowledge that MB molecules can intercalate in DNA duplexes and will remain attached to it<sup>36</sup>.

### 3.5 Changing the Number of Methylene Blue Sites

Other experiments in the lab suggested that decreasing the excess of MB staples can decrease the degree of aggregation. The effect of this on the final structure is that there are not enough strands to fill all the sites, so effectively the origami is labelled with less MB molecules.

A more controlled version of this experiments reduces the number of MB sites by using a smaller number of MB binding extended staples and keeping the excess constant. As a first trial, the number was reduced from 98 to 36, a 2.7x decrease.

This experiment was done using another staple mix already in use in the lab, so that some other differences are present. Specifically the number of surface binding sites is reduced from 30 to 14 and they are extended on the 3' end, instead of the 5' end, so that now the MB and the surface binding tails are located on different sides of the origami, as shown in Figure 3.11. Once the origami is placed on surface, the MB molecules will be on the top side, further from the surface. While this might decrease the signal seen in electrochemistry experiments, it dramatically reduces crowding on the origami surface, from approximately 1 tail per 60 nm to 1 tail per 218 nanom<sup>2</sup> for MB and even less for surface binding sites. The crowding might have prevented the origami from sticking to the surface in previous experiments, as the binding sites might have been inaccessible. Moreover, if the structures stick with a lower amount of surface binding sites, less analyte molecules are necessary for the displacement of each origami. The new design was annealed and did not show significant aggregation up to concentrations of 20 nM, as the gel in Figure 3.12 proves. More so the bands are clear enough that all the structures seem well formed, without significant smear on either side, which, if present, could suggest malformed or aggregated origami. To confirm if the origami is really well formed, AFM imaging was performed on a template stripped gold surface.

This was prepared as explained before (Paragraph ??) and then incubated for one hour

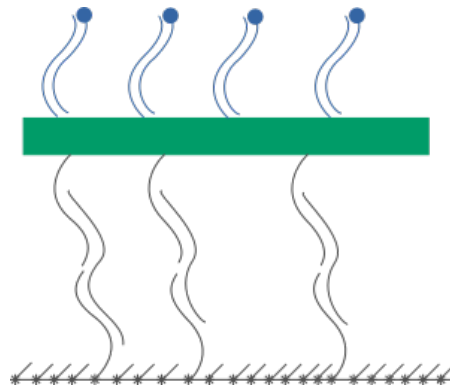


**Figure 3.11** – Revised origami design with 36 MB sites on the 5' end and 14 surface binding sites on the 3' end.

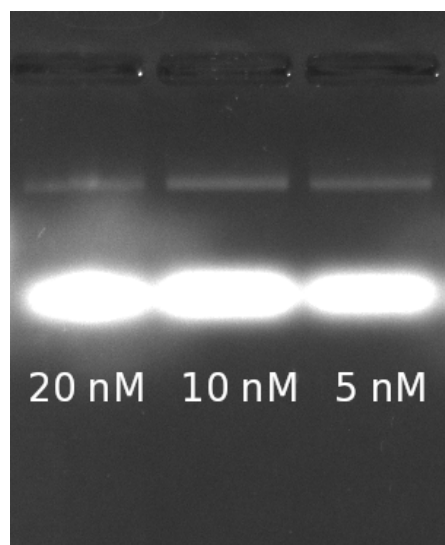
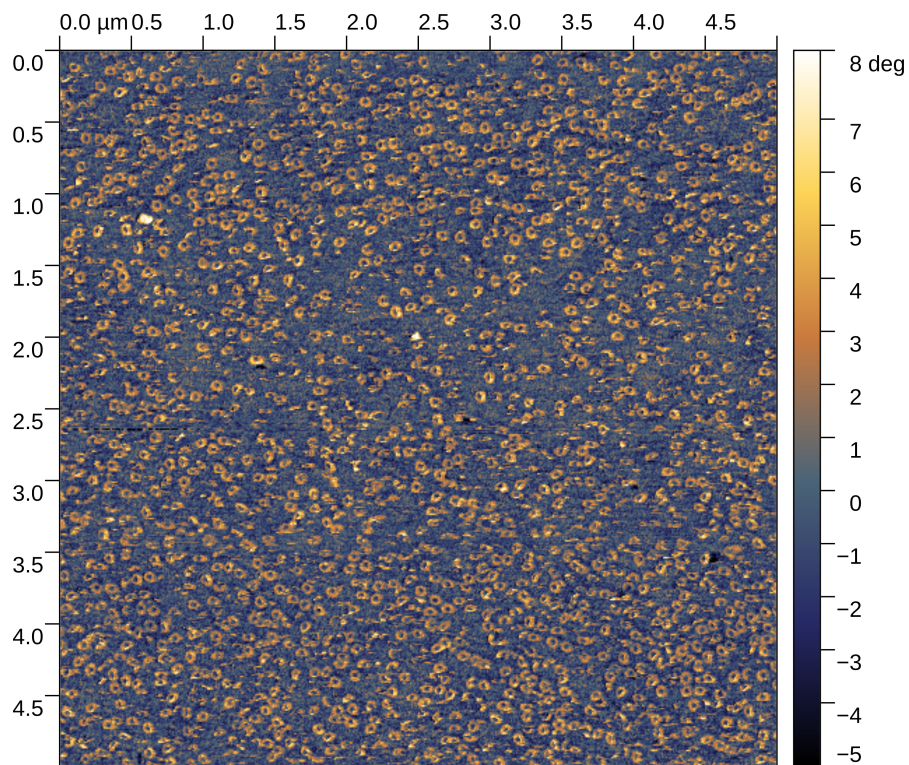


**Figure 3.12** – Agarose gel for an origami design with 36 MB sites on the 5' end and 14 surface binding sites on the 3' end, annealed, from left to right, at a scaffold concentration of 20 nM, 10 nM and 5 nM. The white smear on the left seems due to reflections on the gel, not to difference in the samples.

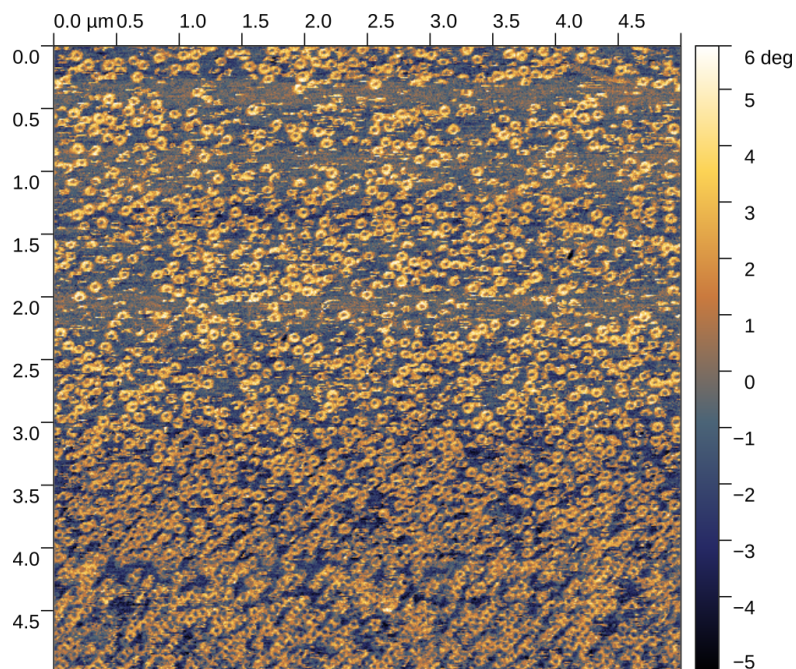
with 300 nM of the thiolated origami binding strands after reducing the thiol with TCEP. After rinsing, the sample was passivated overnight with mercaptohexanol, a step that is not required with AFM, as the aim is to remove oxygen currents in electrochemistry, but important to work in the same conditions that will be applied for the final assembly. The origami were deposited from the 20 nM tube and incubated for thirty minutes before rinsing again with buffer and measuring. Two different samples were actually prepared from two different origami tubes, in order to test the effect of free surface binding strands. The first tube (referred to as “1x” hereon) has DNA origami with the surface binding tails in 1x excess to the staples, in order to prevent free surface binding tails from occupying free sites on the surface and prevent origami binding. The second tube (“10x”) instead has a 10x excess of surface binding tails to the staples, so that a large number of them will be free to fill the oligo sites on the surface. We expect this to reduce the number of origami bound to the surface by virtually deactivating them.

Figure 3.13 shows a 5 by 5  $\mu\text{m}$  area for the 1x sample, as measured in a tapping mode setup on the phase channel. This is useful as the surface roughness of gold drowns the signal from the origami and it is easier to see them on the phase channel where gold features are invisible. While some of the origami are bent or not perfectly circular, they are very close to the design in cadnano and there is no evidence of MB molecules preventing folding. The density, while not reaching full coverage ( $\sim 100$  origami/cm) is high enough that some signal can be expected from electrochemistry (compared to similar densities of EDNA) and imaging in different locations on the same sample reveals even higher density. However there seems to be very little difference for the 10x sample (Figure 3.14), where an even higher density of origami can be observed. There is no real reason to see a higher density here and it is probably due to local differences that depend on the area of the sample measured, but the experiment still disproves the theory proposed earlier that the free surface binding tails will prevent origami binding. We explain this with the high number of thiolated oligos on the surface, which means that there may still be many that are available (not filled by free surface binding oligos) where the origami can still bind.

While these results are promising in terms of labelling DNA origami with methylene blue molecules, subsequent electrochemical measurements, with samples prepared with the same protocol, revealed no signal due to MB redox. This is not surprising as the



**Figure 3.13** – AFM phase imaging of a template stripped gold sample after deposition of the origami design described before, annealed with 1x excess of surface binding sites.



**Figure 3.14** – AFM phase imaging of a template stripped gold sample after deposition of the origami design described before, annealed with 10x excess of surface binding sites.

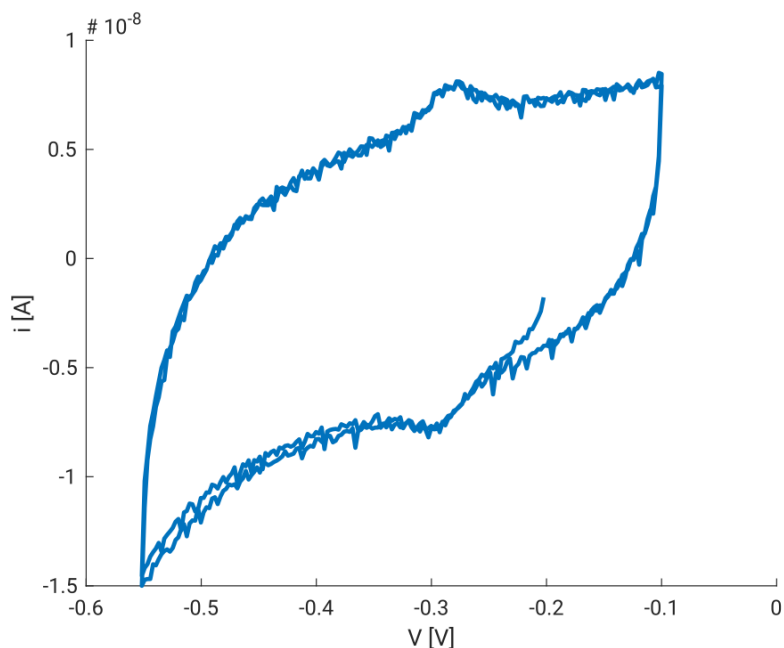


**Figure 3.15** – Cyclic voltammogram of MB labelled origami with 36 sites on a template stripped gold sample. The shielding of background currents is not ideal and the cycle is not well repeated, but around -0.28 V there is a clear increase in signal due to the presence of MB molecules.

redox indicators are located more than 50 bp from the surface and that can be roughly translated to more than 20 nm. This distance might already be too large for electron tunneling and the double stranded DNA does not have the flexibility required to easily bring them closer to the electrode.

To test the hypothesis of inaccessibility of MB molecules from the surface, the origami was redesigned moving the surface binding sites back from the 3' end to the 5' end. While the problem of crowding on the 5' side is now relevant again, the distance from the surface is reduced to a few nanometers, allowing for electron tunneling, possibly faster than EDNA systems.

Also in this case, agarose gel (not shown) confirmed correct origami formation up to 20 nM scaffold concentration. A sample was prepared for electrochemical studies. The two CV cycles shown in Figure 3.15 seem to suggest a bad passivation layer, but this is due only to the lower scale on the y-axis with respect to previous shown EDNA experiments; the baseline absolute value for the passivation layer are comparable. On top of this, both plots in the two directions have apparent bumps do the signal coming from the

---

redox reaction of methylene blue, which can be confirmed by checking the voltage at half distance between the two peaks, located close to -0.28 V. The noise on the experiments is exaggerated by the small y-scale and due to problems with the instrument at the time. Having proved the successful labeling of DNA origami with methylene blue, the next chapter will focus on the use of this device as a DNA sensor and further improvements.



# DNA Origami Electrochemical Sensor

The methylene blue peaks shown in Figure 3.15 are difficult to use to measure probe density by baseline subtraction, as the technique requires a sharp peak to minimize the influence of a non precise baseline extraction. More interesting at this point is the study of electron transfer kinetics in the methylene blue redox reaction, which can give more insight (and validation) on the geometry of the system. The procedure is the one explained in Section 2.4, where square wave voltammetry is performed in a frequency sweep and the peak current is plotted on a Lovrić plot (dividing it by the frequency at which it is measured). Figure 4.1 shows the result of the measurement, with a maximum at 80 Hz, that can be extracted as the electron transfer rate. This suggests that the origami adhere well to the surface, bringing the methylene blue molecules much closer than in EDNA experiments, where the measured electron transfer rate is 13 Hz, around 6 times lower. However, the peak in the Lovrić plot suggests that the number of methylene blue molecules that interact with the electrode is two orders of magnitude lower than previous EDNA samples. Just to evaluate this result, we performed probe density evaluation from the CV measurement, as inaccurate as the the result might be. The two estimates are not far from each other, as the CV measurement yield a density of  $2.4E10$  MB/cm, which is around 50 times lower than EDNA experiments.

This first protocol, while it is able to successfully give a MB signal from DNA origami, is insufficient to be used as a platform to demonstrate the biological sensing capabilities of this system in any meaningful way. In order to do so, density should increase at least one order of magnitude, so that the challenge is to understand why the reading is so low and how to improve this.

The number of  $2.4E10$  MB/cm, divided by 36 (the number of MB molecule per origami),

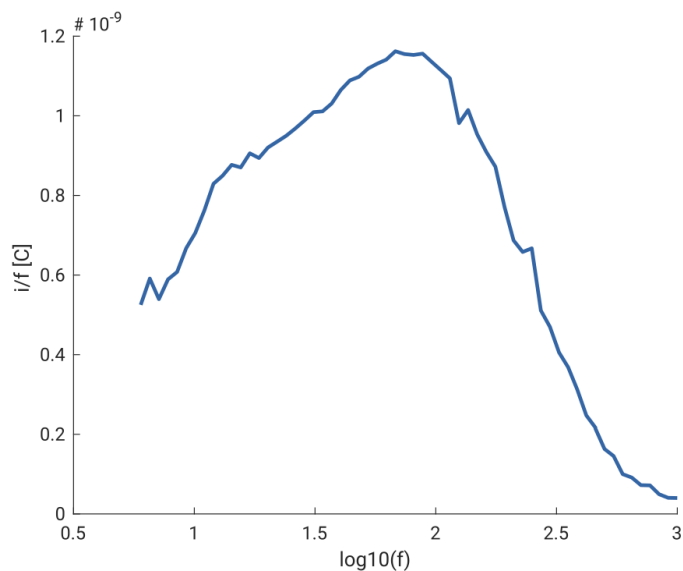


**Figure 4.1** – Lovrić plot of the DNA origami with 36 methylene blue molecules and 14 surface binding sites, on the same sample measured in Figure 3.15.

gives a result of  $6.6E8$  DO/cm (DNA origami per square centimeter), that can be translated to roughly  $7$  DO/ $\mu\text{m}$ , while a single DNA origami should occupy an area of  $10000$  nm, giving a maximum theoretical density of  $100$  DO/ $\mu\text{m}$ . The simplest hypothesis to explain this is that effectively the achieved density of origami is lower than expected and AFM would verify a similar result. Or possibly, some areas, for example in the center of the electrode, might be well coated, while other, at the edges, may have low to no presence of sensing molecules. This idea seems falsified by AFM measurements of previous structures (the flipped DNA origami of Figures 3.13 and 3.14), but new AFM measurements should be repeated on this design. It is entirely possible that the crowding of the surface binding side of the origami (now filled with 14 surface tails and 36 MB tails) might make contact with the surface less effective and hybridization harder.

On the other side it is also possible that another assumption is wrong, that is the fact that 36 MB molecules are measured on each origami. While there is reason to believe that, with sufficient strand excess, almost all origami will be labeled with 36 indicators, they may not be entirely accessible to the electrode for different reasons: some might be too far from the surface, preventing tunneling, or blocked by the crowding of DNA tails.

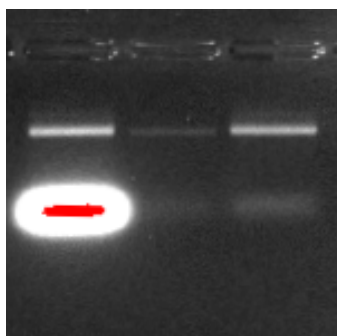


**Figure 4.2** – Agarose gel electrophoresis for a DNA sample with 36 MB molecules before and after five cycles of ultra centrifugation purification (lanes 1 and 3). The second lane is the same sample after 3 cycles, but the brightness is lower for errors when loading the gel in the well. The red spot indicates saturation of the photosensor in the scanner.

#### 4.0.1 Purification

In order to make the experiment more reproducible and eliminate a few variables, the purification of DNA origami was attempted. While purification has always been used to remove unbound staples from DNA origami samples, it is unclear whether the presence of methylene blue could affect the process. Methods based on ion buffer exchange (high performance liquid chromatography) were discarded as the charge on MB molecules would affect the ion exchange and render it useless. Another commonly used technique uses ultra centrifugal filters, where the sample is centrifuged against a membrane that will block the origami and let flow through the staples. However this creates a very high local concentration of origami on the membrane, where MB could cause aggregation and significantly affect recovery of the sample.

To minimize such effect, the filters were used in a situation far from the usual ultra centrifugation, by setting lower rotational speeds ( $2000 \times g$  instead of  $14000 \times g$ ) in a “more gentle” procedure. The original sample is diluted in buffer and spun for 6 min, then new buffer is added and the operation is repeated five times. A gel is run with the original sample and the purified sample (lane 1 and 3 in Figure 4.2, to verify the yield and the removal of staples. The staple band (fuzzy on the lower end) is clearly reduced significantly, although not completely eliminated, while the origami band seems to be preserved and no aggregation is observed at all. The yield is estimated by integrating the brightness of each band origami band and is equal to around 90%, which would be

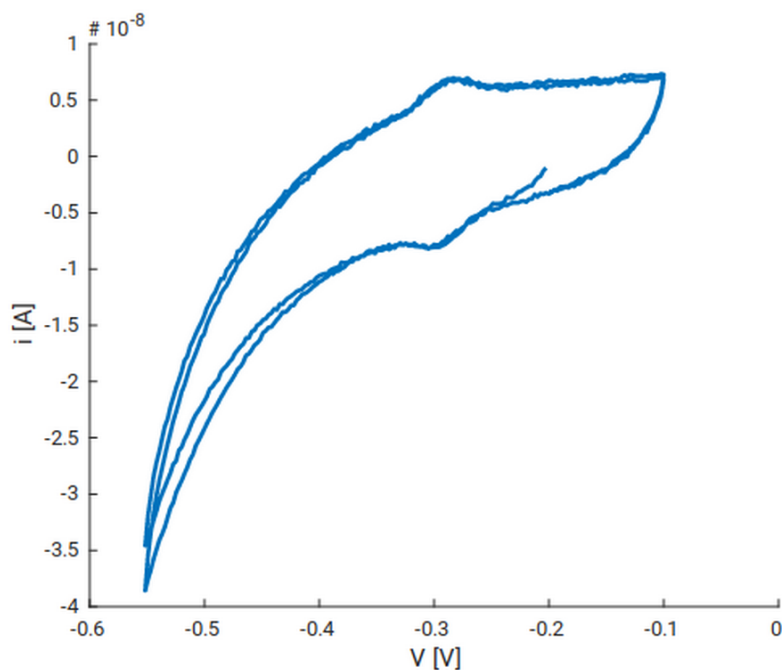


**Figure 4.3** – Cyclic voltammogram of a purified 36 MB origami deposited on a gold electrode after purification. The quality of the passivation layer is degraded in the lower end of the voltage scale, starting to show influence from oxygen currents.

very good for this technique.

Another gold substrate is prepared for electrochemical analysis (deposition of thiolated strand for origami binding and passivation with mercaptohexanol), before depositing on it the purified DNA sample, for two hours. This results in a clear improvement in the final sensor, visible from CV measurements in Figure 4.3. Measuring the density from CV peaks yields however once more a low value, between 9 and 12 DO/ $\mu\text{m}$ , once more far from the theoretical limit. The electron transfer rate from the Lovrić plot (Figure 4.4) is comparable to the first one recorded, but the peak current/frequency is twice as high (compatible with the density) and the general plot seems cleaner, with a sharper peak. The maximum peak height measured during this sweep is 0.36  $\mu\text{A}$  which is still some fraction of EDNA currents, but clearly measurable with commercial systems. Another difference is the absolute position of the peak, located here at 100 Hz, making this system faster than the unpurified one. It is theorized that free staples might be trapped between the origami and the passivation layer in the previous experiment, thus keeping MB molecules further from the surface and reducing the electron transfer rate with lower

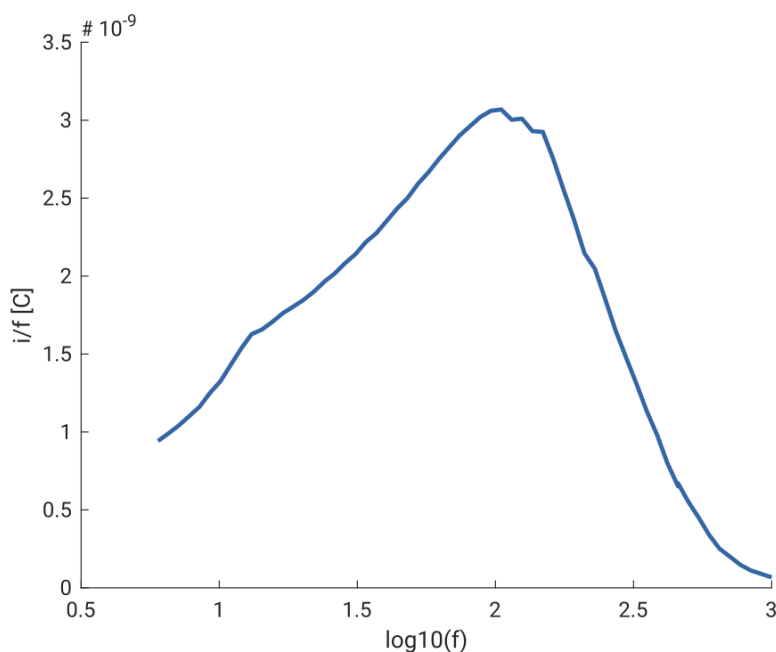


**Figure 4.4** – Lovrić plot of the sample deposited after purification, showing a higher electron transfer rate, peaking at 100 Hz, with higher maximum currents.

tunneling probability.

It is also interesting to note that both Lovrić plots shown in this chapter suggest the presence of a second, slower, MB population located at around 15 Hz. This is deduced from the appearance of a shoulder to the main peak, located around those frequencies, that are also the frequencies of EDNA bound methylene blue. This population seems remarkably smaller than the main one, as it does not really create a second peak, but its presence is not completely understood. It may come from residual single stranded MB tails that are not bound to the origami, or from MB tails that are more difficult to access.

The same sample, after removing the silicone gasket, was prepared for AFM imaging. The gasket removal is a prying off process that can physically impact the gold underneath (it may be cracked or stripped), however careful handling should prevent damage to the origami layer. Figure 4.5 shows one frame from the imaging on a 10 x 10 μm area, that seems densely covered with DNA origami. The estimated density of 40-60 DO/μm from the image is still sub-optimal, but higher than what measured with the electrochemical experiments. Due to the instability of the sample and its frailty, it was not possible

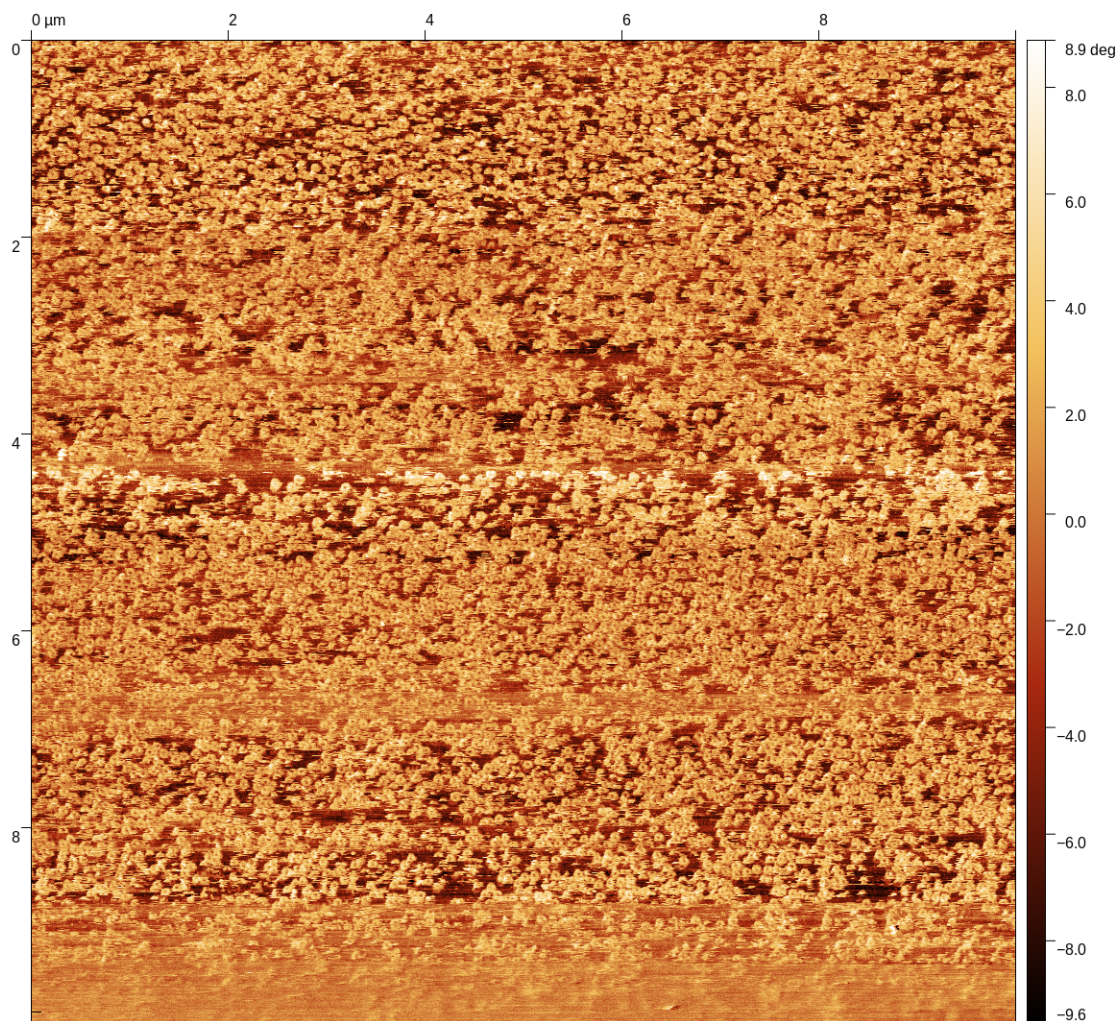


**Figure 4.5** – AFM imaging of the sample in Figures 4.3 and 4.4, after removing the gasket. Due to the unstable imaging conditions, the image is not very clear, but the origami density can be extracted.

to image other areas satisfactorily, so that the doubt remains whether the coating is uniformly dense or sparser on the edges.

## 4.1 Origami Displacement

In order to prove the effectiveness of the DNA origami sensor, it is necessary to test the change in response to the presence of the analyte. We recall that in this proof of concept, the surface binding tails and the thiolated oligos on surface are not perfectly complementary, as there is a 5 nt long sequence on the tails that remains single stranded. This is the

“access point” for the invader, the analyte strand: when added to the system it will start binding here and then it will displace the thiolated strand, substituting it in hybridizing the tails. Once this happens on all the fourteen surface binding sites of the origami, the whole structure will be free from the electrode and will be easily washed away by flushing the cell. An increasing number of such events indicates higher concentrations of analyte and will eventually produce a proportional change in the measured current.

Another sample was prepared with the same procedure and measured under the usual TAE/Mg buffer as in the previous cases. After this, the buffer was exchanged with another TAE/Mg buffer with 300 nM of the invading analyte strand, left overnight to displace as many origami as possible. Then the sample was measured again after exchanging the buffer back to the standard one. Figure 4.6 shows the cyclic voltammograms before and after invasion, while Figure 4.7 shows the alternating current voltammograms for the same setup.

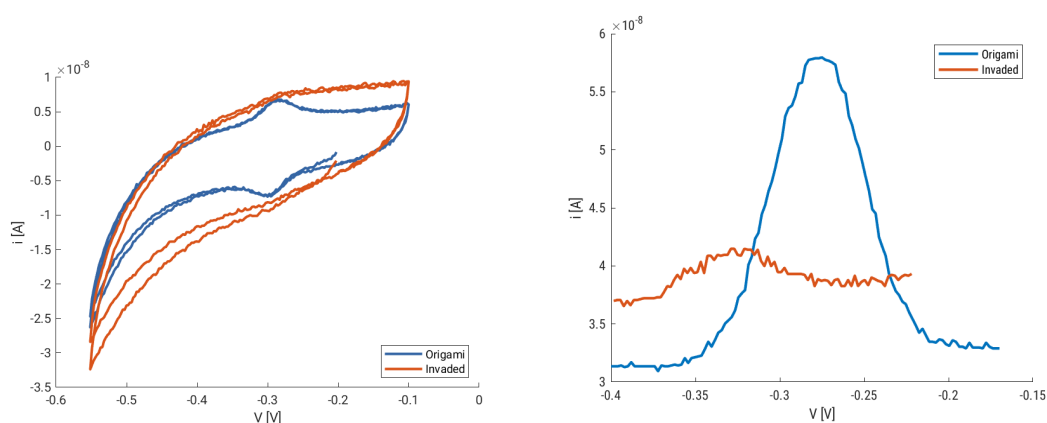


**Figure 4.6** – Cyclic voltammograms before and after invasion of the analyte strand at 300 nM. **Figure 4.7** – Alternating current voltammograms before and after invasion of the analyte strand at 300 nM.

analyze displacement, introduce increase of sites from 36 to 72, concentration of origami with amicon, 1kb linker



## Conclusions

expand

DNA origami is a relatively recent technique, with a history of little more than fifteen years, and during this time many groups have worked on developing it as a toolkit, expanding its capabilities and improving the structural functions. However many have also wondered about real world uses for a technique that allows precise control at a nanometric level, but does not seem to find its killer application. Hopefully this work can add to the exploration of new applications, offering a first demonstration of a DNA origami enabled biological sensor. At the same time, the most interesting section might be the one on methylene blue labeling, which will enable to easily design electrochemically active DNA nanostructures, adding new interaction capabilities to any DNA origami and thus possibly expanding the scope of this technique.

As this work is part of a larger several years long project, the proof of concept shown here is still far from the final flytrap sensor and several obstacles still have to be overcome before reaching the long end goal. Being able to fold larger origami will allow to retain the same design flexibility even for the two part origami, being able to increase the MB loading and possibly change the shape of the top lid to accommodate proteins. Then, selective binding of only one face on gold will be necessary to correctly position the flytrap and have one part free to float before analyte binding. Such advancements will also benefit to the knowledge of DNA origami and they will possibly be reused for new projects.



# Acknowledgements

---

add appendices  
1) shift in lovric  
2) origami on car-  
boxylic acid



# Bibliography

1. Holliday, R. A Mechanism for Gene Conversion in Fungi. *Genetics Research* **5**, 282–304 (1964).
2. Cromie, G. A. *et al.* Single Holliday Junctions Are Intermediates of Meiotic Recombination. *Cell* **127**, 1167–1178 (2006).
3. Chen, J. & Seeman, N. C. Synthesis from DNA of a Molecule with the Connectivity of a Cube. *Nature* **350**, 631–633 (1991).
4. Shih, W. M., Quispe, J. D. & Joyce, G. F. A 1.7-Kilobase Single-Stranded DNA That Folds into a Nanoscale Octahedron. *Nature* **427**, 618–621 (2004).
5. Rothmund, P. W. K. Folding DNA to Create Nanoscale Shapes and Patterns. *Nature* **440**, 297–302 (2006).
6. Douglas, S. M. *et al.* Rapid Prototyping of 3D DNA-Origami Shapes with caDNAno. *Nucleic Acids Research* **37**, 5001–5006 (2009).
7. Qian, L., Soloveichik, D. & Winfree, E. Efficient Turing-Universal Computation with DNA Polymers. *Lecture Notes in Computer Science (including subseries Lecture Notes in Artificial Intelligence and Lecture Notes in Bioinformatics)* **6518 LNCS**, 123–140 (2011).
8. Andersen, E. S. *et al.* Self-Assembly of a Nanoscale DNA Box with a Controllable Lid. *Nature* **459**, 73–76 (2009).
9. Bard, A. J. & Faulkner, L. R. *Electrochemical Methods* 2nd (John Wiley & Sons, Inc., 2000).
10. Vassilev, P. & Koper, M. T. M. Electrochemical Reduction of Oxygen on Gold Surfaces: A Density Functional Theory Study of Intermediates and Reaction Paths. *The Journal of Physical Chemistry C* **111**, 2607–2613 (2007).

11. Fan, C., Plaxco, K. W. & Heeger, A. J. Electrochemical Interrogation of Conformational Changes as a Reagentless Method for the Sequence-Specific Detection of DNA. *PNAS* **100**, 9134–9137 (2003).
12. Xiao, Y., Lubin, A. A., Baker, B. R., Plaxco, K. W. & Heeger, A. J. Single-Step Electronic Detection of Femtomolar DNA by Target-Induced Strand Displacement in an Electrode-Bound Duplex. *Proceedings of the National Academy of Sciences* **103**, 16677–16680 (2006).
13. González-Fernández, E., Avlonitis, N., Murray, A. F., Mount, A. R. & Bradley, M. Methylene Blue Not Ferrocene: Optimal Reporters for Electrochemical Detection of Protease Activity. *Biosensors and Bioelectronics* **84**, 82–88 (2016).
14. Xiao, Y., Piorek, B. D., Plaxco, K. W. & Heeger, A. J. A Reagentless Signal-On Architecture for Electronic, Aptamer-Based Sensors via Target-Induced Strand Displacement. *Journal of the American Chemical Society* **127**, 17990–17991 (2005).
15. Hu, J., Wang, T., Kim, J., Shannon, C. & Easley, C. J. Quantitation of Femtomolar Protein Levels via Direct Readout with the Electrochemical Proximity Assay. *Journal of the American Chemical Society* **134**, 7066–7072 (2012).
16. Arroyo-Currás, N. *et al.* Real-Time Measurement of Small Molecules Directly in Awake, Ambulatory Animals. *Proceedings of the National Academy of Sciences* **114**, 645–650 (2017).
17. Grossi, G., Jepsen, M. D. E., Kjems, J. & Andersen, E. S. Control of Enzyme Reactions by a Reconfigurable DNA Nanovault. *Nature Communications* **8**, 1–8 (2017).
18. Erdem, A., Kerman, K., Meric, B., Akarca, U. S. & Ozsoz, M. Novel Hybridization Indicator Methylene Blue for the Electrochemical Detection of Short DNA Sequences Related to the Hepatitis B Virus. *Analytica Chimica Acta* **422**, 139–149 (2000).
19. Zhang, W., Bas, A. D., Ghali, E. & Choi, Y. Passive Behavior of Gold in Sulfuric Acid Medium. *Transactions of Nonferrous Metals Society of China* **25**, 2037–2046 (2015).

20. Vieu, C. *et al.* Electron Beam Lithography: Resolution Limits and Applications. *Applied Surface Science* **164**, 111–117 (2000).
21. O'Connor, S. D., Olsen, G. T. & Creager, S. E. A Nernstian Electron Source Model for the Ac Voltammetric Response of a Reversible Surface Redox Reaction Using Large-Amplitude Ac Voltages. *Journal of Electroanalytical Chemistry* **466**, 197–202 (1999).
22. Ricci, F., Lai, R. Y., Heeger, A. J., Plaxco, K. W. & Sumner, J. J. *Effect of Molecular Crowding on the Response of an Electrochemical DNA Sensor*
23. White, R. J., Phares, N., Lubin, A. A., Xiao, Y. & Plaxco, K. W. Optimization of Electrochemical Aptamer-Based Sensors via Optimization of Probe Packing Density and Surface Chemistry. *Langmuir : the ACS journal of surfaces and colloids* **24**, 10513 (2008).
24. Steel, A. B., Herne, T. M. & Tarlov, M. J. Electrochemical Quantitation of DNA Immobilized on Gold. *Analytical Chemistry* **70**, 4670–4677 (1998).
25. Lao, R. *et al.* Electrochemical Interrogation of DNA Monolayers on Gold Surfaces. *Analytical Chemistry* **77**, 6475–6480 (2005).
26. Nicholson, R. S. Theory and Application of Cyclic Voltammetry for Measurement of Electrode Reaction Kinetics. *Analytical Chemistry* **37**, 1351–1355 (1965).
27. Dauphin-Ducharme, P., Arroyo-Currás, N. & Plaxco, K. W. High-Precision Electrochemical Measurements of the Guanine-, Mismatch-, and Length-Dependence of Electron Transfer from Electrode-Bound DNA Are Consistent with a Contact-Mediated Mechanism. *Journal of the American Chemical Society* (2019).
28. Dauphin-Ducharme, P. *et al.* Chain Dynamics Limit Electron Transfer from Electrode-Bound, Single-Stranded Oligonucleotides. *The Journal of Physical Chemistry C* **122**, 21441–21448 (2018).
29. Komorsky-Lovrić, Š. & Lovrić, M. Measurements of Redox Kinetics of Adsorbed Azobenzene by “a Quasireversible Maximum” in Square-Wave Voltammetry. *Electrochimica Acta* **40**, 1781–1784 (1995).
30. Komorsky-Lovrić, Š. & Lovrić, M. Square-Wave Voltammetry of Quasi-Reversible Surface Redox Reactions. *Journal of Electroanalytical Chemistry* **384**, 115–122 (1995).

31. Instruments, G. *Square-wave Voltammetry* <https://www.gamry.com/application-notes/physechem/square-wave-voltammetry/> (visited on 06/09/2019).
32. Millipore-Sigma. *16-Mercapto-1-hexadecanol* <https://www.sigmaaldrich.com/catalog/buildingblock/product/matrixscientific/mat047025912?lang=en&region=US> (visited on 02/06/2019).
33. Engelhardt, F. A. S. *et al.* Custom-Size, Functional, and Durable DNA Origami with Design-Specific Scaffolds. *ACS Nano* (2019).
34. Marchi, A. N., Saaem, I., Vogen, B. N., Brown, S. & LaBean, T. H. Toward Larger DNA Origami. *Nano Letters* **14**, 5740–5747 (2014).
35. MIT. *CanDo* <https://cando-dna-origami.org> (visited on 30/07/2019).
36. Kelley, S. O., Barton, J. K., Jackson, N. M. & Hill, M. G. Electrochemistry of Methylene Blue Bound to a DNA-Modified Electrode. *Bioconjugate Chemistry* **8**, 31–37 (1997).